M-current downregulation leads to stellate ganglia sympathetic hyperactivity associated with hypertension

Harvey Davis[1,2*], Neil Herring[1], David J Paterson[1,2**]

1 Burdon Sanderson Cardiac Science Centre, Department of Physiology, Anatomy and Genetics, Sherrington Building, University of Oxford, Oxford, OX1 3PT, UK

2 Wellcome Trust OXION Initiative in Ion Channels and Disease, Department of Physiology, Anatomy and Genetics, Sherrington Building, University of Oxford, Oxford, OX1 3PT, UK

Author contributions H.D performed, interpreted and analyzed all experiments and modelling. H.D produced figures. H.D, N.H and D.J.P wrote and edited the manuscript. H.D, N.H and D.J.P designed the project.

Corresponding authors *Harvey.Davis@gtc.ox.ac.uk, **David.Paterson@dpag.ox.ac.uk

Summary

Cardiac sympathetic nerves are hyperactive in many cardiovascular diseases, however, the mechanisms underlying this are unknown. In humans, this phenotype is known to precede the development of hypertension and contribute to the severity of the disease. We highlight an electrophysiological phenotype in post-ganglionic sympathetic stellate ganglia neurons from prehypertensive spontaneously hypertensive rats (SHR), and use single cell RNA-sequencing, molecular biology, perforated patch-clamp and computational modelling to uncover the underlying mechanism. I_M appears to be transcriptionally downregulated and pharmacological inhibition of I_M in control neurons can recapitulate the SHR phenotype. We also show I_M expression in human stellate ganglia. We demonstrate the contribution of a plethora of I_{Na}, $I_{K,}$ I_{Ca} and I_{Cl} channels in stellate ganglia neuronal firing, alongside a thorough characterization of this physiologically important ganglia. This is the first evidence of cellular electrophysiological hyperactivity in cardiac sympathetic neurons in hypertension and highlights I_{Na} and I_M as targets of interest.

Introduction

Sympathetic hyperactivity is a well-documented co-morbidity that contributes to the etiology of many cardiovascular diseases (Herring, Kalla and Paterson, 2019). For example, in hypertension, increased cardiac sympathetic drive is linked to the development of left ventricular hypertrophy (Schlaich *et al.*, 2003) and subsequent heart failure, which are independent predictors of mortality (Levy *et al.*, 1990).

A significant component of the dysautonomia associated with hypertension resides at the level of the post-ganglionic sympathetic neuron. For example, neurons from the stellate ganglia, which predominately innervate the heart (Pardini, Lund and Schmid, 1989, 1990), have enhanced Ca^{2+} driven (Li *et al.*, 2012; Larsen *et al.*, 2016), norepinephrine release (Shanks, Manou-Stathopoulou, *et al.*, 2013) and impaired re-uptake via NET (Shanks, Mane, *et al.*, 2013). However, both animal models and patients with hypertension also have increased sympathetic nerve firing rate as measured by muscle and renal sympathetic nerve activity (Grassi, 2009a; Manolis *et al.*, 2014). Whether this is centrally driven or results from changes in the excitability of post-ganglionic neurons before the onset of hypertension is unknown.

We therefore characterized the electrophysiological behavior of sympathetic neurons from the stellate ganglia of prehypertensive rats that develop high blood pressure over time (Minami *et al.*, 1989). We undertook single cell RNA-sequencing to identify channel subunit expression in control and disease conditions and used this to guide a comprehensive electrophysiological exploration of their contribution to firing rate. Further to this, we highlighted that key targets were also present in the human stellate ganglia. In particular, we investigated the role of M-current (I_M), sodium current (I_{Na}), T-type calcium current (I_{CaT}),

calcium activated potassium current (I_{KCa}), calcium activated chloride current (I_{CaCC}), hyperpolarization-activated current (I_H), and delayed rectifier potassium current (I_K).

We show that down regulation of M-current causes hyperexcitability in diseased neurons and that this observation is recapitulated in normal neurons when M-current is blocked. Neuronal computational modelling indicates that modulation of I_M alongside I_{Na} availability is a powerful driver of excitability and may present a novel therapeutic target in states of cardiac sympathetic overactivity.

Methods

Animal work declaration Animal use complied with the University of Oxford local ethical guidelines and was in accordance with the Guide for the Care and Use of Laboratory Animals published by the US National Institutes of Health (NIH Publication No. 85-23, revised 2011) and the Animals (Scientific Procedures) Act 1986 (UK). Experiments were performed under British Home Office Project License PPL 30/3131 and P707EB251. All animals were ordered from Envigo and housed on a 12-hour day-night cycle. Animals were sacrificed via an overdose of pentobarbitone and confirmed via exsanguination according to schedule one of the Animals (Scientific Procedures) Act 1986 (UK).

Animals Male normotensive Wistar rats and prehypertensive SHR's were culled at 5-6 weeks of age, at which age SHR's possess a phenotype unaffected by prolonged hypertension as found in older animals. Moreover, around this age post-natal ion channel expression stabilizes in sympathetic ganglia (Hadley *et al.*, 2003)**.**

Human stellate ganglia tissue Stellate ganglia were collected from organ donors at the time of organ procurement as approved by the UCLA IRB: 12-000701. Written informed consent

was provided by the patient or appropriate designee. This study complies with the Declaration of Helsinki.

Cell isolation and culturing Stellate ganglia were dissected and immediately transferred to ice-cold HEPES buffered L15 media (L1518, Thermofisher, US). Ganglia were then cut into 2 mm sections using surgical scissors, and enzymatically digested at 37 ^{o}C first using 1 mg/ml Collagenase IV (Worthington, US) in L15 for 25 minutes, followed by 30 minutes in 2 mg/ml Trypsin (Worthington, US) in Ca^{2+} and Mg^{2+} free Hanks buffered salt solution (Thermofisher, US). Enzymes were then inhibited using two washes of a blocking solution containing 10% FBS. The tissue was then suspended in a plating media containing Neurobasal plus media, B27 plus, 100 ng/ml 2.5s NGF, 25 mM glutamax and 50 units/ml Pen-strep and mechanically disrupted using a fire-blown glass pipette. The cell suspension was then plated onto Poly-D-lysine coated Fluorodish 35 mm dishes (WPI, US), which had been previously incubated for 2 hours with 1 ug/ml laminin, a concentration chosen to allow cell adhesion and survival, but limiting neurite outgrowth (Buettner and Pittman, 1991). The cells were then incubated at 37 ^{o}C with 5% CO_2 for a period of 1-5 days in vitro before use. All datasets were recorded from at least 2 cultures, with each culture requiring 4 animals. Phase contrast microscopy was used to enable neuronal identification. Neurons were identified in dissociated culture based on their large size and circular somata relative to the surrounding cell types.

Electrophysiological Data acquisition All electrophysiological data were acquired using Winwcp (Version 5.4.0) and recorded via a Multiclamp 700B amplifier (Molecular Devices, US) with an axon digidata 1550A (Molecular devices, US) digitizer. All current clamp recordings were sampled at 10 kHz. M-current deactivation curves were sampled at 10 KHz.

Perfusion Cells were constantly perfused at a rate of 5-6 ml/min, drugs were applied via this perfusion system. Most drugs were continuously applied for a duration of 5 minutes before data acquisition, XE-991, substituted LiCl and Linopirdine were perfused for 10 minutes before recording. Recordings were performed at room temperature.

Perforated patch-clamp recordings Amphotericin B (0.48 mg/ml) was used as the perforating agent (Rae *et al.*, 1991), recordings were initiated after low series-resistance electrical access was achieved (<30 MΩ) and stable for a period of five minutes. All voltage clamp recordings used 70% series resistance compensation and capacitance cancellation. Current clamp recordings were bridge balanced. All recordings were monitored throughout, and recordings with R_S changes > 20% were discarded. The external recording solution for both current clamp and voltage clamp recordings was as follows: 5.2 mM KCl, 140 mM NaCl, 1 mM $MgCl_2$, 1.8 mM $CaCl_2$, 10 mM HEPES, 10 mM D-Glucose. External solution pH was adjusted to 7.4 with NaOH. For removal of external calcium, calcium was excluded from this solution and 5 mM EGTA was added. The internal solution was composed as follows: 145 mM K^+-Aspartate, 2.2 mM EGTA, 10 mM HEPES, 1 mM $MgCl_2$. Internal pH was adjusted to 7.3 using KOH.

Whole cell patch-clamp recordings Whole cell action potential recordings with Rs values >12 MΩ discarded. Current clamp recordings were bridge balanced and membrane potentials were corrected for liquid junction potentials. All recordings were monitored throughout, and recordings with R_S changes > 20% were discarded. Single action potentials were evoked via a 10ms positive current injection, at the minimal required injection size. External solution composition was the same as for perforated patch. For LiCl substitution experiments, 140 mM LiCl was substituted for NaCl. The internal solution was as follows: 130 mM K^+-Gluconate, 10

mM KCl, 10 mM HEPES, 10 mM Na^+-Phosphocreatine, 4 mM MgATP, 0.3 mM Na_2GTP. Internal pH was adjusted to 7.3 with KOH.

To study K_{Na}, NaCl was substituted for LiCl to allow an inward g_{Li} via Na_V channels but prevent activation of slick and slack channels by intracellular sodium (Silvana *et al.*, 2003; Kaczmarek *et al.*, 2013). For Ca^{2+} free experiments, Ca^{2+} was removed from the external solution and 5 mM EGTA, a Ca^{2+} buffer, was added.

qRT-PCR Total RNA from whole flash frozen stellate ganglia was isolated using a RNeasy minikit (Qiagen, US) and immediately stored on dry ice before cDNA library preparation. For cDNA synthesis, Superscript IV VILO with ezDNase genomic DNA depletion (Thermofisher, US) was used, cDNA was then stored at -80°C until required. Taqman PCR primers were used for the transcript identification of KCNQ2 (Rn00591249_m1), KCNQ3 (Rn00580995_m1), KCNQ5 (Rn01512013_m1), SCN10A (Rn00568393_m1), where either GAPDH (Rn01775763_g1) or B2M (Rn00560865_m1) were used to normalize values via the ΔΔCT method (Livak and Schmittgen, 2001). Samples were measured on an ABI Prism 7000 (Thermofisher, US) as per the standard protocol for taqman.

Cryosectioning and Immunohistochemistry Freshly isolated stellate ganglia were immediately transferred to 4% paraformaldehyde for 1-2 hours, after which the tissue was incubated overnight in 20% sucrose-PBS at 4 °C, before embedding in OCT compound (Tissue-Tek). Tissue was then frozen and stored at -80 °C until cryosectioning the tissue as 12 µm sections. Slides were then permeabilized in 0.3% triton-X for 30 minutes at room temperature, before blocking for 2 hours in 1% BSA, 5% donkey serum. Sections were then incubated for 24 hours with primary antibodies at 4°C, followed by five 5 minute washes in PBS and 2 hours incubation with the relevant secondary antibodies. Sections were

subsequently washed 3 times in PBS, and incubated with DAPI/PBS for 5 minutes, before a final 2 washes in PBS. Slides were then mounted with 50% glycerol in PBS before imaging. Sections were imaged on a Zeiss LSM 880 Airy Scan Upright laser-scanning confocal microscope with a Plan-Apochromat 20x/0.8 M27 objective. Sections were DAPI stained, labelled with a mouse anti-TH antibody (66334-1-Ig) (ProteinTech, US) and a rabbit antibody against either KCNQ2 (ab22897), KCNQ3 (ab66640) or KCNQ5 (ab66740) (Abcam, UK). For secondary antibodies, 1:200 Donkey anti-mouse Alexa Fluor 555 (A-31570) and 1:200 Donkey anti-rat Alexa Fluor 488 (A-21208) were used (Invitrogen).

Single cell RNA-sequencing A single cell suspension of stellate ganglia cells was prepared via enzymatic dissociation as described under cell culture methods. Following blockade of enzymatic activity via three washes in blocking solution, the cell solution was transferred to phosphate buffered saline. The cell solutions were immediately transferred to ice and transported to the Wellcome Trust Centre for Human Genetics (WTCHG) for single cell sequencing via 10x genomics chromium (10x genomics, US) and Illumina hiseq 4000 (Illumina, US). This approach achieved 66-72K reads per cell, with a sequencing depth of 53-55% and 14-17K mean reads per cell before filtering.

Initial analysis was performed by the WTHCG using the cell ranger pipeline (x10 genomics) with default parameters, before the data were exported to Seurat (v3.0) (Stuart *et al.*, 2019) and analyzed in house. Cells were excluded in Seurat if the number of counts per cell was less than 4000 or percentage of mitochondrial genes was equal to or less than 0.3. For FindVariableFeatures we used 10000 features and the election method VST. Data was intergrated using 30 dimensions, 30 principle components were using for PCA analysis. UMAP and TSNE, FindNeighbours were ran with 19 dimensions. Findclusters was ran with a

resolution of 0.6. Differential expression analysis was performed via MAST(Finak *et al.*, 2015) within Seurat.

Electrophysiological Data analysis Analysis of firing rate data were performed in WinWCP (v5.4.0). M-current deactivation curves were analyzed within Clampfit (v10.7, Molecular Devices, US). Graphs were produced in either Graphpad prism (v8.2.1) or ggplot2 (v3.2.1) and Waffle (v1.0.1) in R (Version 3.5.3). Statistical analysis was performed in GraphPad prism, all relevant datasets were normality tested.

Firing rate was taken as the maximum firing rate elicited by a range of 10 pA current injections between 10-200 pA. Membrane potential was monitored for stability during drug wash in and cells with large jumps in membrane potential were discarded.

Action potential parameters were measured from the first sequential 50 pA current step that induced an action potential. Peak amplitude (mV) was taken as the difference between the average baseline and maximum peak response of the action potential. Action potential upstroke (mV/ms) was taken as the maximum velocity from baseline to the peak amplitude.

Input resistance was calculated based upon a series of hyperpolarizing and depolarizing current injections ranging from -200 to 200 pA in amplitude in 10 pA increments (Spruston and Johnston, 1992). The average value of the final 100 ms was analyzed. As previously classified, small hyperpolarizing pulses were assumed to elicit the least active processes and any points that departed from linearity with these points or contained visible active processes in the final 200 mS of current injection were excluded.

Liquid junction potentials were calculated in JPCalcW (Barry, 1994) in Clampex (v11.0.3) (Molecular Devices, US), where ion availabilities were used instead of concentrations. Free

Ca^{2+}, ATP, EGTA and Mg^{2+} for internal solutions were estimated via MaxChelator (v8) (Bers, Patton and Nuccitelli, 2010) when relevant. For perforated-patch voltage-clamp and current clamp recordings a Liquid junction potential of 24.3 mV was calculated, without correction for the perforated patch Donnan potential (Horn and Marty, 1988). Whole cell current clamp recordings had an estimated liquid junction potential of -15.7 mV.

Computational Modelling Simulations were performed in python (v3.7.4) to script the NEURON environment (v7.7) (Hines and Carnevale, 2001; Hines, Davison and Muller, 2009). I_{Na} and I_k were modelled using the built in Hodgkin-Huxley kinetics. An existing model of I_m was used from ModelDB (McDougal *et al.*, 2017). The cell was morphologically represented by a ball and stick model with a somatic diameter of 22 µM. The simulated dendrites contained only passive currents, had a diameter of 1 µM and a length of 100 µM. The model cell was stimulated by a 0.1 nA current injection at the midpoint of the soma, $soma_{0.5}$, for 1000 ms to elicit a train of action potentials. I_{Na} max amplitude was varied to simulate alterations in I_{Na}. Cell output was recorded from the same midpoint, $soma_{0.5}$. Data was visualized using the Bokeh python library (v1.4.0).

Statistics All datasets were normality tested, except for firing rate, which was taken as a discontinuous variable and treated as non-parametric data. Statistical analysis and normality tests were performed in graphpad prism (v8.2.1). The specific statistical test applied is stated in the figure legends with statistical significance accepted at $p < 0.05$ on two tailed tests.

Results

Stellate ganglia neurons are hyperexcitable in the prehypertensive SHR

Cultured stellate ganglia neurons of the prehypertensive SHR have a significantly higher induced firing rate than neurons cultured from normotensive age matched Wistar neurons as highlighted in Figures 1A and 1B. Of note the firing rate appears to plateau within the stimulation range used (10-200 pA) (Figure 1B). This firing rate difference appears to be time resolved, with the majority of Wistar neurons firing action potentials within only the first 300 ms of stimulation, this phenotype is represented in Figure 1C via a raster plot of 30 Wistar and SHR neurons during a 1000 ms of 150 pA current injection.

We also observed alternate indicators of cellular hyperexcitability. The change in firing rate was accompanied by a 3.065 ± 1.128 mV mean decrease in resting membrane potential between Wistar and SHR neurons (Figure 1D). The rheobase (minimum current injection of duration >300 ms required to reach the action potential threshold) was decreased in SHR neurons as observed via a series of 10 pA current steps of duration 1000 ms in the range 0-200 pA in amplitude (Figure 1E). Input resistance showed a non-significant trend to increase in the SHR (Figure 1F).

The SHR has a higher percentage of tonic firing neurons

Sympathetic neuron firing from other sympathetic and parasympathetic ganglia have been previously characterised into 3 subtypes (Cassell, Clark and McLachlan, 1986; Keast, McLachlan and Meckler, 1993; Wang and McKinnon, 1995; Weigand and Myers, 2010), as represented in Figure 1H. Here these subtypes have been assigned colour codes to allow for a visual representation of the firing rate and time course of firing in a range of conditions

throughout the manuscript. As per previous work (Wang and McKinnon, 1995), Phasic 1 neurons, represent neurons that fire only one action potential for a 1000 ms current injection in the range of 0-200 pA. Phasic 2 neurons fire 2-5 action potentials, all within the first 500 ms of a 1000 ms stimulation pulse for all recordings within the stimulation range 0-200 pA. Tonic neurons fire either greater than 6 action potentials or continue to fire after 500 ms of stimulation of a 1000 ms stimulation pulse within the current injection range 0-200 pA.

When the percentage of neurons conforming to these subtypes is compared between cultured Wistar and cultured SHR neurons, Wistar neurons were found to be predominantly phasic 1 and phasic 2, whereas in the SHR, neurons were predominantly found to be of the tonic subtype (Figure 1I). This data is supported by similar observations in Whole cell patch-clamp recordings (Supplementary Figure 1).

A change in ion channel subunit expression was observed in SHR neurons

Single cell sequencing revealed a heterogenous population of cell clusters in the both Wistar and SHR dissociated stellate ganglia (Figure 2A), which mapped to known cell type markers (Figure 2B; Supplementary Figures 3 and 4) including a large population of cells which are specific for a range of known sympathetic markers (Figure 2C). Differential expression analysis between the Wistar and SHR sympathetic neuron populations identified in Figure 2C highlight a significant decrease in 5 ion channel subunit encoding genes that may contribute to firing rate of stellate ganglia sympathetic neurons (Table 1) (Full list clarified in supplementary 2D).

M-current is conserved and functionally reduced in SHR stellate ganglia neurons

Was a decrease in KCNQ5 subunit expression the most likely explanation for the difference in phenotype? When assessed by RT-qPCR, gene expression of M-current encoding KCNQ2, KCNQ3 and KCNQ5 subunits is decreased in total RNA extracted from whole SHR ganglia (Figure 3A). We also confirmed M-current subunit expression in samples of total RNA taken from human stellate ganglia (Figure 3B). Using immunohistochemistry M-current encoding subunits KCNQ2, KCNQ3 and KCNQ5 were also expressed at a protein level in tyrosine hydroxylase (TH) positive cells (Supplementary Figure 5G), a classic marker for sympathetic neurons.

M-current can be recorded by deactivation curves, in this case applied from a holding potential of -25mV to -55 mV, allowing for a relaxation of current corresponding to I_M. These recordings were made in perforated patch, as I_M is known to rundown in whole cell recordings. To confirm that the current measured was I_M we subtracted and measured current that was inhibited by I_M inhibitor 10 µM XE-991 (Wang *et al.*, 2000; Greene, Kang and Hoshi, 2018). These data were then normalised to cell capacitance. By this measure, I_M was shown to be functionally present in stellate ganglia neurons and to be downregulated in SHR relative to Wistar (Figure 3C).

M-current inhibition increased the excitability of Wistar stellate ganglia neurons

M-current pharmacology was used to assess the role of M-current in firing rate and other electrophysiological parameters in stellate ganglia neurons. M-current inhibition by 3 µM XE-991(Wang *et al.*, 2000; Greene, Kang and Hoshi, 2018) caused a significant increase in Wistar stellate ganglia neuron firing rate, measured as the maximum firing rate of tested neurons within a stimulation range of 0-200 pA (Figure 3D). When this data was visualised as electrophysiological subtypes we observed an increase in tonic neurons after XE-991

application and a reduction in phasic 1 and phasic 2 subtypes (Figure 3K). This is supported by a significantly decreased rheobase (Supplementary figure 5D) and an accompanying depolarisation of resting membrane potential (Supplementary figure 5A).

Similar results were seen after application of 30 µM Linopirdine, an alternative M-current inhibitor at a dose comparable in efficacy to 3 µM XE-991 (Costa and Brown, 1997). Linopirdine increased maximum firing rate in Wistar neurons (Figure 3E). This also caused a reduction in phasic 1 and phasic 2 subtypes, and an increase in tonic neurons (Figure 3H). As with XE-991, Linopirdine also reduced rheobase amplitude (Supplementary figure 5E) and depolarised the resting membrane potential of these neurons (Supplementary Figure 5B).

M-current activation reduced excitability of SHR and Wistar stellate ganglia neurons

As I_M was shown to be reduced, but not entirely absent via 10 µM XE-991-substracted deactivation curves (Figure 3C), we also tested whether increasing SHR M-current via the activator retigabine(Main *et al.*, 2000; Tatulian *et al.*, 2001; Corbin-Leftwich *et al.*, 2016) would be sufficient to reduce firing rate. We found that retigabine significantly reduced SHR stellate ganglia neuron maximum firing rate at all 3 doses tested (Figure 3F). These data are visualised for maximal firing rate as subtypes in Figure 3I, where the number of Tonic neurons decreases, and 4 cells are prevented from firing at 3 µM retigabine in the stimulation range 0-200 pA. These observations were accompanied by a hyperpolarisation of the resting membrane potential of these neurons at all doses tested (Supplementary figure 5C). Retigabine increased rheobase amplitude at 3 µM retigabine in neurons for neurons that still fired within 0-200 pA stimulation (Supplementary Figure 5F), but at higher doses too few neurons still fired in this range to allow for a quantitative comparison of rheobase amplitude.

I_{Na}, SK channels and K_v2.1 also control SHR neuron firing rate

Using single cell RNA-sequencing and a series of pharmacological inhibitors, we screened a range of calcium and voltage-gated ion channels with a known role in determining the firing rate of other neuronal populations. In Figure 4A the patterns of expression for channels implicated in firing rate (Supplementary Figure 2D) are shown against cell clusters highlighted in the Wistar and SHR stellate ganglia (Figure 2A; Figure 2B). For these channels, either 1 or 2 pharmacological inhibitors were applied to SHR neurons to observe any effect on firing rate (Figures 4-5; Table 2). Pharmacological inhibitors which had a significant effect on the firing rate of these neurons are shown in Figures 4-5 and non-significant inhibitors are shown in Table 1.

Low dose (10 nM) Tetrodotoxin (TTX) (Tucker *et al.*, 2012) significantly reduced firing rate in SHR neurons (Figure 4D). In a separate population of SHR neurons, high dose TTX (300 nM) was shown to prevent firing in all tested SHR neurons (Supplementary figure 6F), confirming the absence of a large TTX insensitive I_{Na}.

Two compounds tested, K_v2.1 and K_v2.2 inhibitor, Guangxitoxin (Li *et al.*, 2013) and SK channel inhibitor, Apamin (Kawai and Watanabe, 1986), increased SHR stellate ganglia neuron firing rate (Figures 4B-C). 100 nM Guangxitoxin (Figure 4B) significantly increased SHR firing rate from 10 Hz at baseline to 12 Hz, whereas 200 nM Apamin (Figure 4C) increased median firing rate from 7.5 Hz to 11 Hz. The effect of these inhibitors on firing rate subtypes is shown in Figures 4B-4C, where we observed an increase in phasic 1 and phasic 2 neurons after addition of 100 nM 4,9-Anhydrotetrotoxin (Figure 4E) and an increase in the number of tonic firing neurons after 100 nM Guangxitoxin or 200 nM Apamin addition (Figure 4B-C).

Specific Na_v subunit inhibitors also reduce SHR firing

Using a panel of selective inhibitors, we inhibited Na_V subunits shown to be present in the stellate ganglia via single cell RNA-sequencing (Figure 4A). The $Na_v1.1$ and $Na_v1.3$ inhibitor, ICA-121431 (McCormack *et al.*, 2013), was tested for its effect on SHR stellate ganglia neuron firing rate. 1 µM ICA-121431 significantly reduced SHR firing rate (Figure 5A), and converted a majority of neurons to phasic 1 (Figure 5A). The $Na_v1.2$, $Na_v1.3$ and $Na_v1.5$ inhibitor, phrixotoxin-3 is specific for $Na_v1.2$ at the tested dose, 10 nM, and was therefore utilised as a selective $Na_v1.2$ inhibitor (Bosmans *et al.*, 2006). 10 nM phrixotoxin-3 significantly reduced SHR neuron firing rate (Figure 5B) and prevented tonic firing (Figure 5B).

Inhibition of Nav1.6 by 4,9-Anhydrotetrodotoxin (Rosker *et al.*, 2007) significantly reduced firing of SHR neurons (Figure 5C). We also tested 100 nM 4,9-Anhydrotetrotoxin (Rosker *et al.*, 2007) on XE-991 inhibited Wistar neurons, and found that, similar to in the SHR neurons, it significantly decreased firing rate (Figure 5E) and converted the majority of the tested neurons to phasic 1 (Figure 5D).

The persistent Na_v channel inhibitor riluzole (Urbani and Belluzzi, 2000) inhibited firing in the tested population and reduced most neurons to phasic 1 at the lowest dose tested, 3 µM (Figure 5D).

Membrane depolarisation can limit Na_v availability through increasing Na_V inactivation (Ulbricht, 2005). We ensured the depolarised resting membrane potential observed in the SHR (Figure 1D), did not limit SHR firing rate. To do so we applied a series of negative 1 second current injections in the range -10 to -100 pA followed immediately by a stimulatory 1 second 150 pA current injection. By this method, we found that there was no significant difference between these current steps or a 0 pA control in SHR neurons (Supplementary Figure 6G).

Further to these data, we found that $Na_v1.8$ inhibitors, which have previously been shown to inhibit stellate ganglia function *in vivo* (Yu *et al.*, 2017), are likely to act through this mechanism. 100 nM A803467 (Jarvis *et al.*, 2007) and 300 nM A887826 (Zhang *et al.*, 2010) inhibited firing at tested doses (Supplementary Figure 7A) with no observed change in membrane potential (Supplementary Figure 7C-D). However, a third $Na_v1.8$ inhibitor PF04885614 (1 µM) did not change firing rate (Supplementary figure 7B) or resting membrane potential (Supplementary figure 7E). We also found that $Na_v1.8$ was not present by RT-qPCR (Data not shown) nor single cell RNA-sequencing, an observation supported by previous work in the superior cervical ganglion (SCG) and the lack of TTX insensitive Na_v (Supplementary Figure 6E).

Tonic neurons have less I_M and more I_{Na}

By studying action potential kinetics and I_M density between subtype populations we aimed to gain further insight into the mechanisms behind these subtypes. First, we found that in perforated patch clamp recordings input resistance was higher in tonic neurons than phasic 1 and phasic 2 (Figure 6A).

Indirect measures of I_{Na}, action potential upstroke and action potential amplitude, taken from whole cell recordings of action potentials induced by a threshold 10 ms current injection were used to highlight any differences between subtypes. Whole cell recordings were used to reduce the effect of higher R_s values encountered with perforated patch on action potential kinetics. These data reveal higher I_{Na} in tonic and phasic 2 populations than in phasic 1 as measured by amplitude (Figure 6B) or upstroke (Figure 6C).

Further to these data, by comparing the amplitude of the first and second action potential elicited by a threshold 10 pA 1000 ms current injection, we found that in phasic 2,

but not tonic neurons, there was a significant decrease in the second action potential amplitude (Figure 6D).

We confirmed that these parameters were I_{Na} dependent via the effect of low dose TTX on single action potentials as measured by action potential upstroke in perforated patch (Supplementary Figure 6A) or amplitude (Supplementary Figure 6B).

There were no significant differences in resting membrane potential between the three subtype groups when compared via perforated patch (Figure 6E). However, there was a trend towards a more depolarised resting membrane potential in Phasic 2 and Tonic neurons. When viewed per electrophysiological subtype, we observed significantly less I_M, as determined by deactivation curves, in tonic firing SHR neurons than phasic 2 SHR neurons (Figure 6F).

We also found no significant differences between strains in either measure by whole cell patch clamp recordings of action potential upstroke (Supplementary Figure 6C) or amplitude (Supplementary Figure 6D).

Modelling confirms the roles of I_M and I_{Na}

To confirm that modulation of I_M and I_{Na} could theoretically lead to the three electrophysiological subtypes, we used a simple ball and stick computational model to assess the effects of manipulating I_{Na} and I_M on firing rate (Figure 7). We found that decreasing I_{Na} decreased firing rate (Figures 7A, C, E), and that cells with lower I_{Na} would express either a phasic 2 (Figure 7C) or phasic 1 (Figure 7E) phenotype depending upon the relative amount of $I_{Na.}$ If the model included I_M (Figure 7B, D, F) firing was temporally restricted with relatively high I_{Na} (Figure 7B, D) and had no effect on phasic 1 neurons with low I_{Na} (Figure 7F).

Discussion

Stellate ganglia neurons of the SHR are hyperexcitable

We report three primary novel findings. First, sympathetic stellate ganglia neurons from the prehypertensive SHR are hyperexcitable, which manifests as a higher induced firing rate, depolarised resting membrane potential and reduced rheobase. Secondly, I_M is downregulated in the stellate ganglia neurons of the SHR and this is the causative mechanism for membrane hyperexcitability. Thirdly, hyperexcitability can be curbed either by elevation of remaining I_M or via reduction of I_{Na}, via global inhibition or selective inhibition of $Na_v1.1$-1.3, $Na_v1.6$ or I_{NaP}.

This phenotype of increased induced neuronal firing rate is consistent with the major description of sympathetic nerve hyperactivity in humans (Grassi, 2009b) (Manolis *et al.*, 2014). Together with previously reported elevated membrane calcium conductance (Li *et al.*, 2012; Larsen *et al.*, 2016), this will directly lead to the increased cardiac noradrenaline spill over (Esler, 2000).

Prior models of SHR sympathetic neurons

Previous work in the SHR model of hypertension has reported repetitive firing in SCG neurons, but failed to find a convincing mechanism underlying this phenomenon (Yarowsky and Weinreich, 1985; Jubelin and Kannan, 1990; Robertson and Schofield, 1999). The contemporary view is that this change may be due to changes in I_A, which was reported to be larger in SCG neurons of the SHR (Robertson and Schofield, 1999). However, in the stellate ganglia I_M modulation alone was enough recapitulate the SHR phenotype (Figure 3). This dominant role for I_M is in alignment with reports of I_M in the SCG (Wang and McKinnon, 1995).

Further to this, there were no observed changes in I_A encoding transcript expression by single cell RNA-seq (Figure 2D; Supplementary Figure 2D), which is further supported by assessment of I_A in control SCG, suggesting that I_A is the same between Phasic and Tonic neurons (Wang and McKinnon, 1995).

I_M downregulation causes hyperexcitability

The phenotype observed (Figure 1) fits well with known characteristics of I_M, a channel originally discovered in sympathetic neurons of the superior cervical ganglia (Brown and Adams, 1980). Alongside I_M a plethora of potassium channels have been documented in other sympathetic ganglia (Dixon and McKinnon, 1996) and so we felt it was better to use an unbiased approach to search for a viable target.

As I_M is a slowly activating, and non-inactivating inhibitory K^+ current, it provides a restriction upon firing, but only after its considerable activation period. This fits with both a general increase in firing rate (Figure 1A; Figure 1B), and a time-dependent phenotype (Figure 1C). I_M has a powerful effect on neuronal resting membrane potential, as demonstrated in Supplementary Figure 5A-C, therefore the loss of I_M in the SHR is likely to cause the depolarisation of the resting membrane potential in the SHR (Figure 1D). Notably, reversing this depolarisation on its own does not appear to alter firing rate (Supplementary figure 6F), suggesting this variable does not contribute to the overall phenotype. I_M inhibition also reduces rheobase (Supplementary Figure 5D-E), which again fits with the phenotype observed (Figure 1E).

Prior work has investigated the systemic effect of I_M modulators *in vivo* and found Retigabine to reduce cardiac sympathetic activity in the SHR (Berg, 2016) (Berg, 2018). This would be expected based upon our observation of I_M having a dominant role on stellate

ganglia neuron function *in vitro* (Figure 3) and our transcriptional and functional data highlighting I_M as a powerful driver of hyperactivity in the SHR. In further support of our findings, retigabine has been demonstrated to inhibit noradrenaline release from SCG neurons (Hernandez *et al.*, 2008). Moreover, in a co-culture model of SCG neurons and neonatal cardiomyocytes, retigabine also reduced the action of SCG neurons on cardiomyocytes (Zaika, Zhang and Shapiro, 2011). Finally, human genome wide association studies have found two M-current single nucleotide polymorphisms in KCNQ3 (rs138693040-T) (Méndez-Giráldez *et al.*, 2017) and KCNQ5 (rs12195276-T) (Evangelou *et al.*, 2018) to be significantly associated with variation in the electrocardiographic QT interval and pulse pressure respectively, both variables which are modulated by the sympathetic nervous system.

I_{Na} and stellate ganglia neuron firing

The pattern of expression for Na_v subunits is different to that noted for dorsal root ganglia or central neurons, with a stellate ganglia neuron expression pattern of $Na_v1.1$, $Na_v1.2$, $Na_v1.3$, $Na_v1.6$ and $Na_v1.7$ (Figure 4A). Stellate ganglia neurons therefore express peripheral channel $Na_v1.6$, but lack $Na_v1.8$ and $Na_v1.9$ for which subpopulations of sensory peripheral neurons are notable (Bennett *et al.*, 2019)**.** As observed for other central and peripheral neuron populations, I_{Na} modulation appears to be a powerful regulator of firing rate in SHR stellate ganglia neurons (Figure 4D; Figure 5).

Inhibition of all Nav subunits identified by single cell RNA-sequencing (Figure 4A), apart from Nav1.7, significantly reduced SHR firing (Figure 6). This gives some breadth to the potential mechanism of I_{Na} reduction and allows for the targeting of a range of Nav types to find a tolerable inhibitor. Of interest, thoracic epidural anaesthesia using Na channel blockers such as bupivacaine is used clinically in patients experiencing recurrent, life threatening

ventricular tachycardias to block sympathetically driven arrhythmia as a bridge to ablation or surgical cardiac sympathetic denervation (Herring, Kalla and Paterson, 2019).

The key role of persistent current in stellate ganglia neuron firing is demonstrated by the efficacy of I_{NaP} inhibitor riluzole (Figure 6D), $Na_v1.6$ channels contribute a relatively large persistent current (Herzog *et al.*, 2003) (Smith *et al.*, 1998; Rush, Dib-Hajj and Waxman, 2005; Chen *et al.*, 2008), and so it is possible that riluzole is acting primarily on this channel subtype here. These data highlight that targeting either persistent I_{NaP}, $Na_v1.1$-1.3 or Nav1.6 are viable targets to reduce sympathetic hyperactivity.

$Na_v1.7$ inhibition does not affect firing rate by either tested inhibitor (Table 2). This suggests that $Na_v1.7$ does not contribute to firing rate in the SHR model. $Na_v1.7$ undergoes sustained inactivation, unlike $Na_v1.6$ for example (Bennett *et al.*, 2019), and is therefore less likely to support sustained firing. $Na_v1.7$ inhibitors have been billed as a treatment for neuropathic pain, and have seen much academic and industrial attention. Thus the lack of effect on cardiac sympathetic firing can be regarded as a positive indicator that these compounds are unlikely to have sympathetic side effects.

$Na_v1.1$ (*Scn1a*), $Na_v1.2$ (*Scn2a*) and $Na_v1.7$ (*Scn9a*) are downregulated in the SHR (Table 1), but this does not appear to negatively affect SHR neuron firing rate (Figure 1), action potential amplitude (Supplementary Figure 6D) or action potential upstroke (Supplementary Figure 6C), and it may be concluded that these changes either do not cause a reduction in channel protein or that the reduction in I_{Na} is minimal.

$Na_v1.8$ is not present in stellate ganglia neurons

A803647, an inhibitor of the TTX-resistant Na_v subunit, $Na_v1.8$, has been previously shown to have a powerful inhibitory effect on arrhythmogenesis following stellate ganglia stimulation when applied locally *in vivo* (Yu *et al.*, 2017). This was originally attributed to an effect on stellate ganglia neuron $Na_v1.8$ function, however in our hands, we could not find molecular evidence of its expression (Figure 4A) nor could firing occur after 300nM TTX (Supplementary figure 6F). This is in concordance with prior work from the SCG, which show no transcript expression (Akopian, Sivilotti and Wood, 1996) and a lack of TTX resistance I_{Na} (Schofield and Ikeda, 1988).

Our data, and the mechanisms described within this paper, show that the effect of this inhibitor is likely to be through an off-target reduction of I_{Na}, as shown on a cellular level for A803647 and A887826 in this manuscript (Figure 4A; Supplementary Figure 7). This hypothesis is supported by the similar findings from the autonomic nervous system (Stone *et al.*, 2013). If interpreted in this manner, these data support the findings *in vivo*. We suggest that this would be better targeted through inhibition of one of the Na_v subunits shown to be present by our single cell sequencing analysis or functional work (Figure 4A; Figure 6), rather than through off-target effects of $Na_v1.8$ inhibitors.

Calcium-activated membrane channels in the stellate ganglia

Calcium-activated channels are likely to have a role in defining the tone of SHR neuron firing rates, as shown by the increased firing rate after Apamin inhibition of SK channels. Apamin has reported to increase firing rate in SCG neurons, but to a lesser extent than observed here (Figure 4D), with SCG firing only increased from an anecdotal observation of 1 to 3 Hz (Kawai and Watanabe, 1986). In the SCG, Bk channels have been reported to have a

key role in determining a spiking response to Bradykinin and sensitivity to NGF (Vivas, Kruse and Hille, 2014). Our single-cell RNA-sequencing data supports BK channel expression (Figure 4A) and we observed an increase in action potential width (Data not shown) similar to that previously described in dopamine neurons (Kimm, Khaliq and Bean, 2015). We therefore suggest that BK channels are likely to have a role in the stellate ganglia, but that this may be independent from firing rate.

Overall however, the difference in subtype percentages between Wistar and SHR appears to be largely intact between whole-cell and perforated patch techniques, which would imply that this phenotype is largely independent of intracellular calcium dynamics, as they would be largely disrupted in the whole cell conformation (Shah, 2014)(Figure 1; Supplementary Figure 1). We also found no expression differences for calcium-activated channels encoding genes in our single-cell RNA-sequencing dataset (Figure 2D). Further to this, removal of extracellular calcium had a highly variable effect on SHR neuron firing rate, and no net difference in firing rate before and after calcium removal (Table 2).

The calcium activated chloride channel, TMEM16A, does not appear to be involved in determining stellate ganglia neuron firing rate, nor does it appear to be present in the neuronal population (Table 2). This contrasts with the mouse SCG where the use of the broad-spectrum chloride channel inhibitor, 9-AC appeared to reduce firing rate (Martinez-Pinna *et al.*, 2018). It is unknown if this results from the difference in pharmacological inhibitor and methodology or from inter-ganglia and inter-species expression differences, but our electrophysiological and single cell sequencing appear to support each other in our study of the rat stellate ganglia.

K_v2.1, K_{Na}, T-type and HCN currents in neurons of the stellate ganglia

Prior studies have reported the importance of K_v2.1 conductance in the SCG, with a similar effect of inhibiting K_v2.1 to that observed here in the stellate ganglia (Table 2) (Malin and Nerbonne, 2002; Liu and Bean, 2014).

Slick and slack channel encoding transcripts were detected by our single-cell RNA-sequencing, however, we found that substitution of Na^+ for Li^+ which should ablate the majority of the current through K_{Na}, had little effect on firing rate (Table 2). This could suggest the effect of removing K_{Na} was below the detectable limit in our model, or that K_{Na} has a minor role.

Interestingly, T-type calcium, was absent in these neurons, with no effect of 2 selective inhibitors, TTA-A2 (Kraus *et al.*, 2010) and TTA-P2 (Choe *et al.*, 2011), (Table 2) alongside a negative result in the neuronal population via single-cell sequencing (Figure 2C). Prior knockout studies of T-type subunits suggest that these channels regulate the cardiac sympathetic innervation via central pathways (Hansen, 2014), with our data confirming that the role of T-type channels in cardiac sympathetic activity is restricted to central input.

HCN channels appear to be expressed in stellate ganglia neurons via single cell RNA-sequencing (Figure 2C) but appear to have little control over somatic firing properties when tested via either ZD7288 or Ivabradine (Table 2). It is possible that these channels have a larger role in determining stellate ganglia neuron neurite electrophysiology, as observed in central neurons (Shah, 2014), or that these channels are relatively inactive with resting cyclic

nucleotide levels and the relatively depolarised resting membrane potentials observed for these neurons (Figure 1D).

Comparison with other ganglia

Differences between the stellate ganglia and other sympathetic ganglia have now been reported by several measures including NET transporter activity (Shanks, Mane, *et al.*, 2013), input resistance (Wang and McKinnon, 1995; Luther and Birren, 2009) and firing rate subtypes(Wang and McKinnon, 1995; Jobling and Ian L. Gibbins, 1999). As the stellate ganglia provides the majority of cardiac sympathetic innervation, it is important that these data also describe the electrophysiological phenotype of the stellate ganglia as it is currently not characterised.

A range of firing subtypes from Phasic 1 dominant to Tonic dominant have been reported in other ganglia from control models (Keast, McLachlan and Meckler, 1993). It was interesting to observe the presence of all 3 subtypes in the stellate ganglia, as in the SCG only Phasic 1 and Phasic 2 neurons were observed (Wang and McKinnon, 1995). In the coeliac (~58%) and superior mesenteric ganglia (~85%) (Wang and McKinnon, 1995), a higher percentage of tonic neurons have been observed than we observed in the stellate ganglia (Figure 1H; ~20%). We observed that neurons of the Wistar stellate ganglia have a much larger input resistance (218.2 MΩ) in comparison to the majority of measurements from SCG (Mouse 109.7 MΩ, 75-85 MΩ; Rat 389.9 MΩ), Thoracic (Mouse 117.9 MΩ) and Coeliac (Mouse 161.9 MΩ; Guinea pig 116.9 MΩ) ganglia (Jobling and Ian L Gibbins, 1999; Anderson, Jobling and Gibbins, 2001; Lamas, Reboreda and Codesido, 2002; Martinez-Pinna *et al.*, 2018). However, some of this difference may be attributed to interspecies differences.

Previous studies have also observed more depolarised resting membrane potentials for the range of studied sympathetic ganglia, with our estimated value in Wistar of -68.04 mV being more hyperpolarised than most recordings from other ganglia including the SCG (Mouse SCG -49.9 mV, -54 mV; Rat SCG -58.3 mV) (Jobling and Gibbins, 1999)(Lamas, Reboreda and Codesido, 2002)(Martinez-Pinna et al., 2018).

Electrophysiological subtypes of the sympathetic nervous system are dynamic

Stellate ganglia neuron phasic 1 neurons are likely to have low I_{Na} compared to phasic 2 and tonic neurons, which would limit sustained firing (Figure 5; Figure 7). The difference between phasic 2 and tonic neurons is likely to be lower I_M with a spectrum of current amplitudes and associated firing rates.

In other ganglia, a relationship between reduced I_M and tonic firing has been reported (Wang and McKinnon, 1995; Jia *et al.*, 2008; Luther and Birren, 2009) which we have now related to a disease context. I_{Na} has been reported to be higher in tonic firing SCG neurons (Luther and Birren, 2009), however this study provides the first non-correlative evidence that this is crucial for a tonic or phasic 2 phenotype.

Alongside I_M and I_{Na} it is likely that other excitatory or inhibitory channels will shape this relationship in the stellate ganglia, including, but not limited to SK channels and $K_v2.1$. Interestingly, input resistance was not reported to be different between phasic and tonic neurons in prior work (Wang and McKinnon, 1995), but this might be as phasic 1 and phasic 2 neurons were grouped together for this prior study.

The relative ease of pharmacologically converting these neural subtypes (Figures 3-5), suggests they are fluid and dynamic, and therefore do not correspond to hardwired neuron

subtypes. This is supported by our single cell sequencing data, where although three populations of sympathetic neurons appear (Figure 2B), our initial probing into these data suggest that these groupings do not correlate with I_M or I_{Na} expression (Data not shown). There is no evidence at this time that these transcriptome-based groups are in any way related to electrophysiological subtype as suggested by a prior study in related ganglia, where neurochemical content did not appear to correlate with electrophysiology (Keast, McLachlan and Meckler, 1993). These transcriptome defined groups merit further study, but a detailed comparison is beyond the scope of this project.

Limitations

Whilst downregulation of I_M provides an explanation for membrane hyperactivity, we have not identified a pathway by which this may occur. One possible explanation is that this results from continual presynaptic input, contributing to ganglionic LTP (Alkadhi *et al.*, 2001; Alzoubi, Aleisa and Alkadhi, 2010). Also, it is possible that other channels may be contributing to this phenotypic difference, but as the measured variables all correlate well with our observations of I_M inhibition in Wistar neurons, it seems highly likely that I_M downregulation is a major cause.

The SHR model of hypertension has several issues, primarily its reliance on rodent physiology, which differs in several respects from man (Hasenfuss, 1998) and the genetic basis of the SHR pathology, which in humans only appears to contribute but not define hypertensive pathology. To address translatability of our work, we have confirmed that I_M subunits are expressed in human stellate ganglia (Figure 3B), but we have not been able to functionally confirm this. In relation to disease pathology, we use the SHR here as a model of sympathetic nerve hyperactivity, which like in humans, correlates with cardiovascular

disease. In this work we study sympathetic hyperactivity outside of the context of the development of SHR hypertension and chose this model due to its reliable presentation of sympathetic dysfunction.

Electrophysiological studies in this paper were performed at room temperature, due to the poor stability and viability of patch clamping these neurons at physiological temperatures in culture.

Single cell sequencing was the best approach for this study, as bulk sequencing would also incorporate contaminating cell types, for example vascular cells which are known to have ion channel expression changes in the SHR (Jepps *et al.*, 2011) and may therefore confound results. It should be noted that we observed downregulation of all three M-current encoding subunits via RT-qPCR, but only downregulation of KCNQ5 by single cell RNA-sequencing. For KCNQ2, this may be as the detected expression level of KCNQ2 is relatively low via single cell RNA-sequencing (Figure 2C), and therefore any chance is unlikely to be detected. For both KCNQ2 and KCNQ3 it is possible that downregulation of contaminating vascular SHR KCNQ2 and KCNQ3 is detected by our RT-qPCR of the whole stellate ganglion. Regardless, all these data support a downregulation of I_M in stellate ganglia neurons of the SHR, with a functional reduction of I_M supporting this.

Conclusions

We have described in detail a phenotype of sympathetic hyperactivity in stellate ganglia neurons of the SHR and have provided an electrophysiological framework for this observation, guided by single-cell RNA-sequencing of the stellate ganglia and human validation of key transcripts. Targeting key ion channels in the stellate ganglia, such as M-

current, may provide a reversible therapeutic opportunity to treat cardiac sympathetic hyper-responsiveness over and above interventions like surgical stellectomy.

Figure 1 Stellate ganglia neurons of the spontaneously hypertensive rat have a hyperactive phenotype with membrane current dysfunction as observed by perforated patch clamp recordings. (A) Example traces showing the response of sympathetic neurons from control Wistar and pre-hypertensive SHR rats to 150 pA of current injection for a duration of 1000 ms. (B) Median response of Wistar (Black) and SHR (Red) neurons to a range of current injections (Wistar, n = 66; SHR, n = 69) (Mixed-effects model, $p < 0.0001$). (C) Time course of induced firing following a 1000 ms 150 pA current injection in 30 example Wistar and SHR neurons. (D) A significant decrease in the resting membrane potential was observed in SHR neurons (Mean ± SEM) (Wistar, -68.04 ± 0.81 mV, n = 89; SHR, -64.97 ± 0.78 mV, n = 97) (Unpaired t-test, p = 0.0072). (E) A significant decrease in rheobase was observed in SHR neurons (Median ± IQR) (Wistar, 50 pA, n = 70; SHR, 30 pA, n = 70) (Mann-Whitney test, p = 0.0013). (F) A non-significant trend to increased input resistance was observed between Wistar and SHR neurons (Median ± IQR) (Wistar, 218.2 MΩ, n = 26; SHR, 251.8 MΩ, n = 63) (Mann Whitney test, p = 0.066). (G) Examples of sympathetic neuron firing rates by their classical nomenclature, the colour scheme used to indicate these subtypes throughout the article are indicated by a colored square. (H) A trend towards tonic firing neurons was observed in the SHR, shown as percentage of cells conforming to each subtype (Wistar, n = 66; Phasic 1 n = 29, Phasic 2 n = 24, Tonic n = 13; SHR, n = 73; Phasic 1 n = 9, Phasic 2 n = 17, Tonic n = 47).

Figure 2 Single cell RNA-sequencing on Wistar and SHR populations reveals dysregulation of channel subunit expression in SHR stellate ganglia neurons. (A) Single cell RNA-sequencing reveals multiple clusters of cell transcriptomes. (B) These cell clusters align to multiple cell types, as defined using the best-known markers for these cell types. (C) Markers used for sympathetic neurons are shown to be primarily expressed in sympathetic neurons.

Table 1 Differential expression analysis of key ion channels in Wistar vs SHR neurons reveals a number of ion channel subunits are downregulated at transcriptional level in the SHR. Differential expression analysis was performed using MAST in the Seurat package.

Figure 3 M-current is downregulated at a functional level in the stellate ganglia, and pharmacological manipulation of M-current can reverse or induce the firing rate phenotype observed in the SHR. (A) RT-qPCR reveals a downregulation of KCNQ2, KCNQ3 and KCNQ5 expression in the left stellate ganglia of 5-6 week old prehypertensive SHR (Median) (Percentage decrease; KCNQ2, 62.73%; KCNQ3, 35.16%; KCNQ5, 45.88%) (Wistar, n = 4; SHR, n = 3). (B) KCNQ2, KCNQ3 and KCNQ5 subunit expression was confirmed in patient samples of stellate ganglia, taken from donors (Median) (ΔCt; KCNQ2, 11.78; KCNQ3, 8.259; KCNQ5, 10.03; n = 4). (C) M-current density was revealed to be decreased in the SHR as determined by a decrease in XE-991 sensitive current, via a step protocol from -20 mV to -50 mV (Median ± IQR) (Wistar, -4.032 pA/pF, n = 11; SHR, -1.770 pA/pF, n = 9) (Mann-Whitney test, p = 0.0074). (D) M-current inhibition by 3 µM XE-991 significantly increased maximum firing rate induced by current injections in the range 10-200 pA (Median) (Control, 3 Hz; Treated, 7 Hz) (Wilcoxon Test, n = 12, p = 0.0059). (E) M-current inhibition by the alternate inhibitor 30 µM Linopridine also induced a significant increase in firing rate (Median) (Control, 1 Hz; Treated, 5 Hz) (Wilcoxon Test, n = 8, p = 0.016). (F) M-current activation in SHR neurons by retigabine

significantly reduced maximum firing rate at all tested doses (Median) (Control, 5 Hz; 3 µM Retigabine, 1 Hz; 10 µM Retigabine, 0 Hz; 30 µM Retigabine, 0 Hz) (Friedman Test, n = 13, p<0.0001) (Dunn's Multiple comparisons; Control vs 3 µM, p = 0.018; Control vs 10 µM, p = 0.0002; Control vs 30 µM, p < 0.0001). (G)(H) A graphical representation of subtype changes following the application of M-current inhibitors 3 µM XE-991 and 30 µM Linopiridine in Wistar neurons. A trend towards a predominantly tonic firing subtype was observed in both cases. (I) A graphical representation of the effect of M-current activator Retigabine on SHR firing rate, which prevents firing in a third of tested neurons (Grey squares).

Figure 4 Single cell RNA-sequencing and a panel of pharmacological inhibitors were used to determine remaining channels involved in SHR enhanced firing, that may be targetable for the reduction of aberrant sympathetic hyperactivity or key to the SHR sympathetic pathology. (A) Single cell RNA-sequencing was used to identify the cell specific expression patterns of a range of channel subunits which are typically implicated in the control of firing rate in other neuronal populations. (B) Kv2.1 inhibition by 100 nM Guanigotoxin (GxTx)significantly increased maximum firing rate in SHR neurons (Median) (Control, 10 Hz; Treated, 12 Hz) (Wilcoxon test, n = 8, p = 0.039). (C) SK channel inhibition by 200 nM apamin caused a significant increase in firing rate (Median) (Control, 7.5 Hz; Treated, 11 Hz) (Wilcoxon test, n = 8, p = 0.016). (D) Generally targeting TTX-sensitive I_{Na} by 10 nM TTX caused a significant decrease in firing rate (Median) (Control, 2 Hz; 10 nM, 1Hz) (Wilcoxon test, n = 14, p = 0.0078).

Figure 5 Exploring the role of Na_V subunits in SHR firing rate. The effect of specific Na_V subunit inhibitors was investigated in SHR stellate ganglia neurons, and firing rate was found to be targetable through multiple subunits and mechanisms. (A) $Na_v1.1$ inhibition by 1 µM ICA-121431 in SHR neurons significantly reduced maximum firing rate in SHR neurons (Median)

(Control, 4 Hz; Treated, 1 Hz) (Wilcoxon test, n = 9, p = 0.0039). (B) $Na_v1.2$ inhibition by 10 nM Phrixotoxin-3 in SHR neurons significantly reduced maximum firing rate in SHR neurons (Median) (Control, 4.5 Hz; Treated, 2 Hz) (Wilcoxon test, n = 8, p = 0.0313). (C) Nav1.6 inhibition by 100 nM 4,9-Anhydrotetrodotoxin significantly reduced maximum firing rate in SHR neurons (Median) (Control, 12 Hz; Treated, 3 Hz) (Wilcoxon test, n = 13, p = 0.0015). (D) INaP inhibition by 3-10 µM Riluzole in SHR neurons reduced firing rate (Median) (Control, 16 Hz; 3 µM, 1 Hz; 10 µM, 1 Hz; Washout, 12.5 Hz) (Friedman test, n = 8, p < 0.0001) (Dunn's multiple comparisons test; Control vs 3 µM, p = 0.003; Control vs 10 µM, p = 0.007). (E) Nav1.6 inhibition significantly reduced firing rate in M-current (3 µM XE-991) inhibited Wistar neurons (Median) (Control, 2 Hz; XE-991 treated, 3 Hz; XE-991 and 4,9-Anhydrotetrotoxin treated, 1 Hz) (Friedman test, n = 10, p = 0.0084) (Dunn's Multiple comparisons test; XE-991 treated vs XE-991 + 4,9-Anhydrotetrotoxin, p = 0.038).

Table 2 Effect of other channel inhibitors on SHR neuron firing rate. All channels included are non-significant for all stated current injection amplitudes (50, 100, 150 pA or maximum firing rate in response to any 10 pA current step between 0-200 pA). All tested by Wilcoxon tests.

Figure 6 Tonic neurons have lower I_M density and more I_{Na}, both facilitating higher firing rates. (A) Input resistance was significantly higher in tonic neurons than in phasic 2 and phasic 1 neurons (Median ± IQR) (Phasic 1, 166.5 MΩ, n = 18; Phasic 2, 218.2 MΩ, n = 22; Tonic, 279 MΩ, n = 48) (Kruskal-Wallis test; p = 0.0006) (Dunn's multiple comparisons test; Phasic 1 vs Tonic, p = 0.011; Phasic 2 vs Tonic, p = 0.046). (B) Upstroke velocity for phasic 1, phasic 2 and tonic neurons revealed a higher Tonic velocity (Median ± IQR) (Phasic 1, 34.71 mV/ms, n = 20; Phasic 2, 63.65 mV/ms, n = 32; Tonic, 85.38 mV/ms, n = 37) (Kruskal-Wallis test; p = 0.0018) (Dunn's multiple comparisons test; Phasic 1 vs Tonic, p = 0.0012). (C) Action potential

amplitude was significantly higher for phasic 2 and tonic neurons than in phasic 1 neurons (Mean ± SEM) (Phasic 1, 68.30 ± 4.49 mV, n = 21; Phasic 2, 78.25 ± 2.25 mV, n = 32; Tonic, 81.96 ± 2.14mV, n = 37) (One-way ANOVA; p = 0.0071) (Holm-sidak's multiple comparisons test; Phasic 1 vs Phasic 2, p = 0.049; Phasic 1 vs Tonic, p = 0.0054). (D) The amplitude of the second action potential in a train was lower in phasic 2 neurons, but not tonic suggesting an inability to support repetitive firing in phasic 2 neurons (Mean ± SEM) (Phasic 1, First AP 86.67 ± 2.48 mV, n = 25; Phasic 2, First AP 87.34 ± 3.8 mV, Second AP 67.76 ± 4.58 mV, n = 16; Tonic, First AP 93.67 ± 3.22 mV, Second AP 85.52 ± 6.48mV, n = 22) (Multiple t-test's; Phasic 2, p = 0.0026; Tonic, p = 0.22).(E) Resting membrane potential for the three electrophysiological subtypes (Mean ± SEM) (Phasic 1, -63.43 ± 1.38 mV, n = 37 ; Phasic 2, -60.88 ± 1.07 mV, n = 51; Tonic, -59.62 ± 0.96mV, n = 63) (One-way ANOVA, p = 0.065). (F) M-current density was lower in Tonic firing neurons than phasic 2 neurons (Median±IQR) (Phasic 1, -4.09 pA/pF, n=7; Phasic 2, -7.18 pA/pF, n=12; Tonic, -2.62 pA/pF, n=18) (Kruskal-Wallis test; p = 0.0019) (Dunn's multiple comparisons test; Phasic 2 vs Tonic, p = 0.0012).

Figure 7 Simple modelling using a kinetic model of M-current and Hodgkin-Huxley derived I_{Na} and I_K, to study the response to a 1000ms current injection, which confirms the contribution of both I_{Na} and I_M to firing rate subtypes. The model uses a ball and stick configuration, with passive currents only used for an abstract dendritic compartment. Vertical scale bars indicate 40 mV, horizontal scale bars indicate 200 ms. (A) A simulation of high (0.12 S/cm^2) HH derived I_{Na} without I_M. (B) A simulation of high (0.12 S/cm^2) HH derived I_{Na} with I_M. (C) A simulation of reduced (0.118 S/cm^2) HH derived I_{Na} without I_M. (D) A simulation of reduced (0.118 S/cm^2) HH derived I_{Na} with I_M. (E) A simulation of reduced (0.115 S/cm^2) HH derived I_{Na} without I_M. (F) A simulation of reduced (0.115 S/cm^2) HH derived I_{na} with M-current.

Acknowledgements We acknowledge The High-Throughput Genomics Group at the Wellcome Trust Centre for Human Genetics for producing the single cell RNA-sequencing data and for the initial cell-ranger analysis. We acknowledge the British Heart Foundation (RG/17/14/33085) and the Wellcome trust OXION programme and Medical sciences Doctoral training centre, University of Oxford (BST0008Z) for funding this work. NH is supported by a British Heart Foundation Intermediate Fellowship (FS/15/8/3115). We would like to acknowledge Olujimi A. Ajijola and his team for providing human stellate ganglia for this study.

References

Akopian, A. N., Sivilotti, L. and Wood, J. N. (1996) "A tetrodotoxin-resistant voltage-gated sodium channel expressed by sensory neurons," *Nature*, 379(6562), pp. 257–262. doi: 10.1038/379257a0.

Alkadhi, K. A. *et al.* (2001) "Inhibition of ganglionic long-term potentiation decreases blood pressure in spontaneously hypertensive rats," *Experimental Biology and Medicine*, 226(11), pp. 1024–1030. doi: 10.1177/153537020122601109.

Alzoubi, K. H., Aleisa, A. M. and Alkadhi, K. A. (2010) "In vivo expression of ganglionic long-term potentiation in superior cervical ganglia from hypertensive aged rats," *Neurobiology of Aging*. Elsevier, 31(5), pp. 805–812. doi: 10.1016/J.NEUROBIOLAGING.2008.06.007.

Anderson, R. L., Jobling, P. and Gibbins, I. L. (2001) "Development of Electrophysiological and Morphological Diversity in Autonomic Neurons," *Journal of Neurophysiology*. American Physiological SocietyBethesda, MD , 86(3), pp. 1237–1251. doi: 10.1152/jn.2001.86.3.1237.

Barry, P. H. (1994) "JPCalc, a software package for calculating liquid junction potential corrections in patch-clamp, intracellular, epithelial and bilayer measurements and for correcting junction potential measurements," *Journal of Neuroscience Methods*, 51(1), pp. 107–116. doi: https://doi.org/10.1016/0165-0270(94)90031-0.

Bennett, D. L. *et al.* (2019) "The Role of Voltage-Gated Sodium Channels in Pain Signaling," *Physiological Reviews*. American Physiological Society, 99(2), pp. 1079–1151. doi: 10.1152/physrev.00052.2017.

Berg, T. (2016) "M-currents (Kv7.2-7.3/KCNQ2-KCNQ3) Are Responsible for Dysfunctional Autonomic Control in Hypertensive Rats.," *Frontiers in physiology*. Frontiers Media SA, 7, p. 584. doi: 10.3389/fphys.2016.00584.

Berg, T. (2018) "Kv7(KCNQ)-K+-Channels Influence Total Peripheral Resistance in Female but Not Male Rats, and Hamper Catecholamine Release in Hypertensive Rats of Both Sexes.," *Frontiers in physiology*. Frontiers Media SA, 9, p. 117. doi: 10.3389/fphys.2018.00117.

Bers, D. M., Patton, C. W. and Nuccitelli, R. (2010) “Chapter 1 - A Practical Guide to the Preparation of Ca2+ Buffers,” in Whitaker, M. B. T.-M. in C. B. (ed.) *Calcium in Living Cells*. Academic Press, pp. 1–26. doi: https://doi.org/10.1016/B978-0-12-374841-6.00001-3.

Bosmans, F. *et al.* (2006) “Four Novel Tarantula Toxins as Selective Modulators of Voltage-Gated Sodium Channel Subtypes,” *Molecular Pharmacology*, 69(2), pp. 419 LP – 429. doi: 10.1124/mol.105.015941.

Brown, D. A. and Adams, P. R. (1980) “Muscarinic suppression of a novel voltage-sensitive K+ current in a vertebrate neurone,” *Nature*. Nature Publishing Group, 283(5748), pp. 673–676. doi: 10.1038/283673a0.

Buettner, H. M. and Pittman, R. N. (1991) “Quantitative effects of laminin concentration on neurite outgrowth in vitro,” *Developmental Biology*, 145(2), pp. 266–276. doi: https://doi.org/10.1016/0012-1606(91)90125-M.

Cassell, J. F., Clark, A. L. and McLachlan, E. M. (1986) “Characteristics of phasic and tonic sympathetic ganglion cells of the guinea-pig.,” *The Journal of physiology*. Wiley-Blackwell, 372, pp. 457–83. Available at: http://www.ncbi.nlm.nih.gov/pubmed/2425087 (Accessed: September 6, 2018).

Chen, Y. *et al.* (2008) “Functional properties and differential neuromodulation of Na(v)1.6 channels,” *Molecular and cellular neurosciences*. 2008/05/20, 38(4), pp. 607–615. doi: 10.1016/j.mcn.2008.05.009.

Choe, W. *et al.* (2011) “TTA-P2 is a potent and selective blocker of T-type calcium channels in rat sensory neurons and a novel antinociceptive agent,” *Molecular pharmacology*. 2011/08/05. The American Society for Pharmacology and Experimental Therapeutics, 80(5), pp. 900–910. doi: 10.1124/mol.111.073205.

Corbin-Leftwich, A. *et al.* (2016) “Retigabine holds K_V 7 channels open and stabilizes the resting potential,” *The Journal of General Physiology*, 147(3), pp. 229–241. doi: 10.1085/jgp.201511517.

Costa, A. M. N. and Brown, B. S. (1997) “Inhibition of M-current in cultured rat superior cervical ganglia by linopirdine: Mechanism of action studies,” *Neuropharmacology*, 36(11–12), pp. 1747–1753. doi: 10.1016/S0028-3908(97)00155-X.

Dixon, J. E. and McKinnon, D. (1996) “Potassium Channel mRNA Expression in Prevertebral and Paravertebral Sympathetic Neurons,” *European Journal of Neuroscience*. John Wiley & Sons, Ltd (10.1111), 8(1), pp. 183–191. doi: 10.1111/j.1460-9568.1996.tb01179.x.

Esler, M. (2000) “The sympathetic system and hypertension*,” *American Journal of Hypertension*, 13(S4), pp. 99S-105S. doi: 10.1016/S0895-7061(00)00225-9.

Evangelou, E. *et al.* (2018) “Genetic analysis of over 1 million people identifies 535 new loci associated with blood pressure traits,” *Nature Genetics*, 50(10), pp. 1412–1425. doi: 10.1038/s41588-018-0205-x.

Finak, G. *et al.* (2015) “MAST: a flexible statistical framework for assessing transcriptional changes and characterizing heterogeneity in single-cell RNA sequencing data,” *Genome biology*. BioMed Central, 16, p. 278. doi: 10.1186/s13059-015-0844-5.

Grassi, G. (2009a) “Assessment of sympathetic cardiovascular drive in human hypertension: Achievements and perspectives,” *Hypertension*, 54(4), pp. 690–697. doi: 10.1161/HYPERTENSIONAHA.108.119883.

Grassi, G. (2009b) “Assessment of sympathetic cardiovascular drive in human hypertension: Achievements and perspectives,” *Hypertension*, 54(4), pp. 690–697. doi: 10.1161/HYPERTENSIONAHA.108.119883.

Greene, D. L., Kang, S. and Hoshi, N. (2018) “XE991 and Linopirdine are state-dependent inhibitors for Kv7/KCNQ channels that favor activated single subunits.” doi: 10.1124/jpet.117.241679.

Hadley, J. K. *et al.* (2003) “Stoichiometry of expressed KCNQ2/KCNQ3 potassium channels and subunit composition of native ganglionic M channels deduced from block by tetraethylammonium.,” *The Journal of neuroscience : the official journal of the Society for Neuroscience*. Society for Neuroscience, 23(12), pp. 5012–9. doi: 10.1523/JNEUROSCI.23-12-05012.2003.

Hansen, P. B. L. (2014) “Functional importance of T-type voltage-gated calcium channels in the cardiovascular and renal system: news from the world of knockout mice,” *American Journal of Physiology-Regulatory, Integrative and Comparative Physiology*. American Physiological Society, 308(4), pp. R227–R237. doi: 10.1152/ajpregu.00276.2014.

Hasenfuss, G. (1998) “Animal models of human cardiovascular disease, heart failure and hypertrophy,” *Cardiovascular Research*, 39(1), pp. 60–76. doi: 10.1016/S0008-6363(98)00110-2.

Hernandez, C. C. *et al.* (2008) “Regulation of neural KCNQ channels: signalling pathways, structural motifs and functional implications.,” *The Journal of physiology*. Wiley-Blackwell, 586(7), pp. 1811–21. doi: 10.1113/jphysiol.2007.148304.

Herring, N., Kalla, M. and Paterson, D. J. (2019) “The autonomic nervous system and cardiac arrhythmias: current concepts and emerging therapies,” *Nature Reviews Cardiology*. doi: 10.1038/s41569-019-0221-2.

Herzog, R. I. *et al.* (2003) “Distinct repriming and closed-state inactivation kinetics of Nav1.6 and Nav1.7 sodium channels in mouse spinal sensory neurons,” *The Journal of physiology*. 2003/07/03. Blackwell Science Inc, 551(Pt 3), pp. 741–750. doi: 10.1113/jphysiol.2003.047357.

Hines, M. L. and Carnevale, N. T. (2001) “Neuron: A Tool for Neuroscientists,” *The Neuroscientist*. SAGE Publications Inc STM, 7(2), pp. 123–135. doi: 10.1177/107385840100700207.

Hines, M. L., Davison, A. P. and Muller, E. (2009) “NEURON and Python,” *Frontiers in neuroinformatics*. Frontiers Research Foundation, 3, p. 1. doi: 10.3389/neuro.11.001.2009.

Horn, R. and Marty, A. (1988) “Muscarinic activation of ionic currents measured by a new whole-cell recording method.,” *The Journal of General Physiology*, 92(2), pp. 145 LP – 159. doi: 10.1085/jgp.92.2.145.

Jarvis, M. F. *et al.* (2007) “A-803467, a potent and selective Nav1.8 sodium channel blocker, attenuates neuropathic and inflammatory pain in the rat,” *Proceedings of the National Academy of Sciences of the United States of America*. 2007/05/02. National Academy of Sciences, 104(20), pp. 8520–8525. doi: 10.1073/pnas.0611364104.

Jepps, T. *et al.* (2011) “Downregulation of Kv7.4 Channel Activity in Primary and Secondary Hypertension,” *Circulation*. American Heart Association, 124(5), pp. 602–611. doi: 10.1161/CIRCULATIONAHA.111.032136.

Jia, Z. *et al.* (2008) “NGF inhibits M/KCNQ currents and selectively alters neuronal excitability in subsets of sympathetic neurons depending on their M/KCNQ current background.,” *The Journal of*

general physiology. The Rockefeller University Press, 131(6), pp. 575–87. doi: 10.1085/jgp.200709924.

Jobling, P. and Gibbins, Ian L. (1999) “Electrophysiological and Morphological Diversity of Mouse Sympathetic Neurons,” *Journal of Neurophysiology*. American Physiological SocietyBethesda, MD , 82(5), pp. 2747–2764. doi: 10.1152/jn.1999.82.5.2747.

Jobling, P. and Gibbins, Ian L (1999) “Electrophysiological and Morphological Diversity of Mouse Sympathetic Neurons,” *Journal of Neurophysiology*. American Physiological Society, 82(5), pp. 2747–2764. doi: 10.1152/jn.1999.82.5.2747.

Jubelin, B. C. and Kannan, M. S. (1990) “Neurons from neonatal hypertensive rats exhibit abnormal membrane properties in vitro,” *American Journal of Physiology-Cell Physiology*. American Physiological Society Bethesda, MD, 259(3), pp. C389–C396.

Kaczmarek, L. K. *et al.* (2013) “Review Article Slack, Slick, and Sodium-Activated Potassium Channels,” *Article ID*. Hindawi Publishing Corporation ISRN Neuroscience, 2013, p. 14. doi: 10.1155/2013/354262.

Kawai, T. and Watanabe, M. (1986) “Blockade of Ca-activated K conductance by apamin in rat sympathetic neurones,” *British Journal of Pharmacology*, 87(1), pp. 225–232. doi: 10.1111/j.1476-5381.1986.tb10175.x.

Keast, J. R., McLachlan, E. M. and Meckler, R. L. (1993) “Relation between electrophysiological class and neuropeptide content of guinea pig sympathetic prevertebral neurons.,” *Journal of neurophysiology*. American Physiological Society Bethesda, MD , 69(2), pp. 384–94. doi: 10.1152/jn.1993.69.2.384.

Kimm, T., Khaliq, Z. M. and Bean, B. P. (2015) “Differential Regulation of Action Potential Shape and Burst-Frequency Firing by BK and Kv2 Channels in Substantia Nigra Dopaminergic Neurons,” *The Journal of neuroscience : the official journal of the Society for Neuroscience*. Society for Neuroscience, 35(50), pp. 16404–16417. doi: 10.1523/JNEUROSCI.5291-14.2015.

Kraus, R. L. *et al.* (2010) “In Vitro Characterization of T-Type Calcium Channel Antagonist TTA-A2 and In Vivo Effects on Arousal in Mice,” *Journal of Pharmacology and Experimental Therapeutics*, 335(2), pp. 409 LP – 417. doi: 10.1124/jpet.110.171058.

Lamas, A. J., Reboreda, A. and Codesido, V. (2002) “Ionic basis of the resting membrane potential in cultured rat sympathetic neurons,” *NeuroReport*, 13(5). Available at: https://journals.lww.com/neuroreport/Fulltext/2002/04160/Ionic_basis_of_the_resting_membrane_potential_in.10.aspx.

Larsen, H. E. *et al.* (2016) “Dysregulation of Neuronal Ca2+ Channel Linked to Heightened Sympathetic Phenotype in Prohypertensive States.,” *The Journal of neuroscience : the official journal of the Society for Neuroscience*. Society for Neuroscience, 36(33), pp. 8562–73. doi: 10.1523/JNEUROSCI.1059-16.2016.

Levy, D. *et al.* (1990) “Prognostic Implications of Echocardiographically Determined Left Ventricular Mass in the Framingham Heart Study,” *New England Journal of Medicine*. Massachusetts Medical Society, 322(22), pp. 1561–1566. doi: 10.1056/NEJM199005313222203.

Li, D. *et al.* (2012) *Abnormal Intracellular Calcium Homeostasis in Sympathetic Neurons From Young Prehypertensive Rats*, *Hypertension*. doi: 10.1161/HYPERTENSIONAHA.111.186460.

Liu, P. W. and Bean, B. P. (2014) “Kv2 Channel Regulation of Action Potential Repolarization and Firing Patterns in Superior Cervical Ganglion Neurons and Hippocampal CA1 Pyramidal Neurons,” *The Journal of Neuroscience*, 34(14), pp. 4991 LP – 5002. doi: 10.1523/JNEUROSCI.1925-13.2014.

Livak, K. J. and Schmittgen, T. D. (2001) “Analysis of Relative Gene Expression Data Using Real-Time Quantitative PCR and the 2−ΔΔCT Method,” *Methods*, 25(4), pp. 402–408. doi: 10.1006/meth.2001.1262.

Li, X. (Nina) *et al.* (2013) “The Role of Voltage-Gated Potassium Channels Kv2.1 and Kv2.2 in the Regulation of Insulin and Somatostatin Release from Pancreatic Islets,” *Journal of Pharmacology and Experimental Therapeutics*, 344(2), pp. 407 LP – 416. doi: 10.1124/jpet.112.199083.

Luther, J. A. and Birren, S. J. (2009) “p75 and TrkA signaling regulates sympathetic neuronal firing patterns via differential modulation of voltage-gated currents,” *The Journal of neuroscience : the official journal of the Society for Neuroscience*. Society for Neuroscience, 29(17), pp. 5411–5424. doi: 10.1523/JNEUROSCI.3503-08.2009.

Main, M. J. *et al.* (2000) “Modulation of KCNQ2/3 potassium channels by the novel anticonvulsant retigabine,” *Molecular Pharmacology*, 58(2), pp. 253–262. doi: 10.1124/mol.58.2.253.

Malin, S. A. and Nerbonne, J. M. (2002) “Delayed rectifier K+ currents, IK, are encoded by Kv2 alpha-subunits and regulate tonic firing in mammalian sympathetic neurons.,” *The Journal of neuroscience : the official journal of the Society for Neuroscience*. Society for Neuroscience, 22(23), pp. 10094–105. doi: 10.1523/JNEUROSCI.22-23-10094.2002.

Manolis, A. J. *et al.* (2014) “Sympathetic overactivity in hypertension and cardiovascular disease.,” *Current vascular pharmacology*, 12(1), pp. 4–15. Available at: http://www.ncbi.nlm.nih.gov/pubmed/23905597 (Accessed: September 5, 2018).

Martinez-Pinna, J. *et al.* (2018) “A Calcium-Dependent Chloride Current Increases Repetitive Firing in Mouse Sympathetic Neurons.,” *Frontiers in physiology*. Frontiers Media SA, 9, p. 508. doi: 10.3389/fphys.2018.00508.

McCormack, K. *et al.* (2013) “Voltage sensor interaction site for selective small molecule inhibitors of voltage-gated sodium channels,” *Proceedings of the National Academy of Sciences of the United States of America*. 2013/07/01. National Academy of Sciences, 110(29), pp. E2724–E2732. doi: 10.1073/pnas.1220844110.

McDougal, R. A. *et al.* (2017) “Twenty years of ModelDB and beyond: building essential modeling tools for the future of neuroscience,” *Journal of Computational Neuroscience*, 42(1), pp. 1–10. doi: 10.1007/s10827-016-0623-7.

Minami, N. *et al.* (1989) “AGE-RELATED CHANGES IN BLOOD PRESSURE, HEART RATE AND BAROREFLEX SENSITIVITY IN SHR,” *Clinical and Experimental Pharmacology and Physiology*, 16, pp. 85–87. doi: 10.1111/j.1440-1681.1989.tb02999.x.

Pardini, B. J., Lund, D. D. and Schmid, P. G. (1989) “Organization of the sympathetic postganglionic innervation of the rat heart,” *Journal of the Autonomic Nervous System*. Elsevier, 28(3), pp. 193–201. doi: 10.1016/0165-1838(89)90146-X.

Pardini, B. J., Lund, D. D. and Schmid, P. G. (1990) “Innervation patterns of the middle cervical - stellate ganglion complex in the rat,” *Neuroscience Letters*, 117(3), pp. 300–306. doi: https://doi.org/10.1016/0304-3940(90)90681-X.

Rae, J. *et al.* (1991) “Low access resistance perforated patch recordings using amphotericin B,” *Journal of Neuroscience Methods*, 37(1), pp. 15–26. doi: https://doi.org/10.1016/0165-0270(91)90017-T.

Robertson, W. P. and Schofield, G. G. (1999) “Primary and adaptive changes of A-type K+ currents in sympathetic neurons from hypertensive rats,” *American Journal of Physiology-Regulatory, Integrative and Comparative Physiology*. American Physiological Society, 276(6), pp. R1758–R1765. doi: 10.1152/ajpregu.1999.276.6.R1758.

Rosker, C. *et al.* (2007) “The TTX metabolite 4,9-anhydro-TTX is a highly specific blocker of the Nav1.6 voltage-dependent sodium channel,” *American Journal of Physiology-Cell Physiology*. American Physiological Society, 293(2), pp. C783–C789. doi: 10.1152/ajpcell.00070.2007.

Rush, A. M., Dib-Hajj, S. D. and Waxman, S. G. (2005) “Electrophysiological properties of two axonal sodium channels, Nav1.2 and Nav1.6, expressed in mouse spinal sensory neurones,” *The Journal of physiology*. 2005/03/10. Blackwell Science Inc, 564(Pt 3), pp. 803–815. doi: 10.1113/jphysiol.2005.083089.

Schlaich, M. P. *et al.* (2003) “Relation between cardiac sympathetic activity and hypertensive left ventricular hypertrophy,” *Circulation*, 108(5), pp. 560–565. doi: 10.1161/01.CIR.0000081775.72651.B6.

Schofield, G. G. and Ikeda, S. R. (1988) “Sodium and calcium currents of acutely isolated adult rat superior cervical ganglion neurons,” *Pflügers Archiv*, 411(5), pp. 481–490. doi: 10.1007/BF00582368.

Shah, M. M. (2014) “Cortical HCN channels: function, trafficking and plasticity,” *The Journal of physiology*. 2014/04/22. BlackWell Publishing Ltd, 592(13), pp. 2711–2719. doi: 10.1113/jphysiol.2013.270058.

Shanks, J., Manou-Stathopoulou, S., *et al.* (2013) “Cardiac sympathetic dysfunction in the prehypertensive spontaneously hypertensive rat,” *American Journal of Physiology-Heart and Circulatory Physiology*. American Physiological Society, 305(7), pp. H980–H986. doi: 10.1152/ajpheart.00255.2013.

Shanks, J., Mane, S., *et al.* (2013) “Ganglion-Specific Impairment of the Norepinephrine Transporter in the Hypertensive Rat,” *Hypertension*, 61(1), pp. 187–193. doi: 10.1161/HYPERTENSIONAHA.112.202184.

Silvana, F. *et al.* (2003) “Na+-Activated K+ Current Contributes to Postexcitatory Hyperpolarization in Neocortical Intrinsically Bursting Neurons,” *Journal of neurophysiology*, 89, pp. 2101–2111. doi: 10.1152/jn.00695.2002.

Smith, M. R. *et al.* (1998) “Functional analysis of the mouse Scn8a sodium channel,” *The Journal of neuroscience : the official journal of the Society for Neuroscience*. Society for Neuroscience, 18(16), pp. 6093–6102. doi: 10.1523/JNEUROSCI.18-16-06093.1998.

Spruston, N. and Johnston, D. (1992) “Perforated patch-clamp analysis of the passive membrane properties of three classes of hippocampal neurons,” *Journal of Neurophysiology*. American Physiological Society, 67(3), pp. 508–529. doi: 10.1152/jn.1992.67.3.508.

Stone, A. J. *et al.* (2013) “Attenuation of autonomic reflexes by A803467 may not be solely caused by blockade of NaV 1.8 channels,” *Neuroscience letters*. 2013/03/21, 543, pp. 177–182. doi: 10.1016/j.neulet.2013.03.015.

Stuart, T. *et al.* (2019) “Comprehensive Integration of Single-Cell Data,” *Cell*. Elsevier, 177(7), pp. 1888-1902.e21. doi: 10.1016/j.cell.2019.05.031.

Tatulian, L. *et al.* (2001) “Activation of expressed KCNQ potassium currents and native neuronal M-type potassium currents by the anti-convulsant drug retigabine.,” *The Journal of neuroscience : the official journal of the Society for Neuroscience*. Society for Neuroscience, 21(15), pp. 5535–45. doi: 10.1523/JNEUROSCI.21-15-05535.2001.

Tucker, K. R. *et al.* (2012) “Pacemaker Rate and Depolarization Block in Nigral Dopamine Neurons: A Somatic Sodium Channel Balancing Act,” *The Journal of Neuroscience*, 32(42), pp. 14519 LP – 14531. doi: 10.1523/JNEUROSCI.1251-12.2012.

Ulbricht, W. (2005) “Sodium Channel Inactivation: Molecular Determinants and Modulation,” *Physiological Reviews*. American Physiological Society, 85(4), pp. 1271–1301. doi: 10.1152/physrev.00024.2004.

Urbani, A. and Belluzzi, O. (2000) “Riluzole inhibits the persistent sodium current in mammalian CNS neurons,” *European Journal of Neuroscience*. John Wiley & Sons, Ltd (10.1111), 12(10), pp. 3567–3574. doi: 10.1046/j.1460-9568.2000.00242.x.

Vivas, O., Kruse, M. and Hille, B. (2014) “Nerve Growth Factor Sensitizes Adult Sympathetic Neurons to the Proinflammatory Peptide Bradykinin,” *The Journal of Neuroscience*, 34(36), pp. 11959 LP – 11971. doi: 10.1523/JNEUROSCI.1536-14.2014.

Wang, H. S. *et al.* (2000) “Molecular basis for differential sensitivity of KCNQ and I(Ks) channels to the cognitive enhancer XE991,” *Molecular Pharmacology*, 57(6), pp. 1218–1223. Available at: http://www.molpharm.org (Accessed: June 28, 2018).

Wang, H. S. and McKinnon, D. (1995) “Potassium currents in rat prevertebral and paravertebral sympathetic neurones: control of firing properties.,” *The Journal of physiology*. Wiley-Blackwell, 485 (Pt 2)(Pt 2), pp. 319–35. Available at: http://www.ncbi.nlm.nih.gov/pubmed/7666361 (Accessed: May 14, 2018).

Weigand, L. A. and Myers, A. C. (2010) “Synaptic and membrane properties of parasympathetic ganglionic neurons innervating mouse trachea and bronchi,” *American journal of physiology. Lung cellular and molecular physiology*. 2010/01/29. American Physiological Society, 298(4), pp. L593–L599. doi: 10.1152/ajplung.00386.2009.

Yarowsky, P. and Weinreich, D. (1985) “Loss of accommodation in sympathetic neurons from spontaneously hypertensive rats.,” *Hypertension*. Am Heart Assoc, 7(2), pp. 268–276.

Yu, L. *et al.* (2017) “Blocking the Nav1.8 channel in the left stellate ganglion suppresses ventricular arrhythmia induced by acute ischemia in a canine model,” *Scientific Reports*, 7(1), p. 534. doi: 10.1038/s41598-017-00642-6.

Zaika, O., Zhang, J. and Shapiro, M. S. (2011) “Functional role of M-type (KCNQ) K^+ channels in adrenergic control of cardiomyocyte contraction rate by sympathetic neurons.,” *The Journal of physiology*. Wiley-Blackwell, 589(Pt 10), pp. 2559–68. doi: 10.1113/jphysiol.2010.204768.

Zhang, X.-F. *et al.* (2010) “A-887826 is a structurally novel, potent and voltage-dependent Nav1.8 sodium channel blocker that attenuates neuropathic tactile allodynia in rats,” *Neuropharmacology*, 59(3), pp. 201–207. doi: https://doi.org/10.1016/j.neuropharm.2010.05.009.

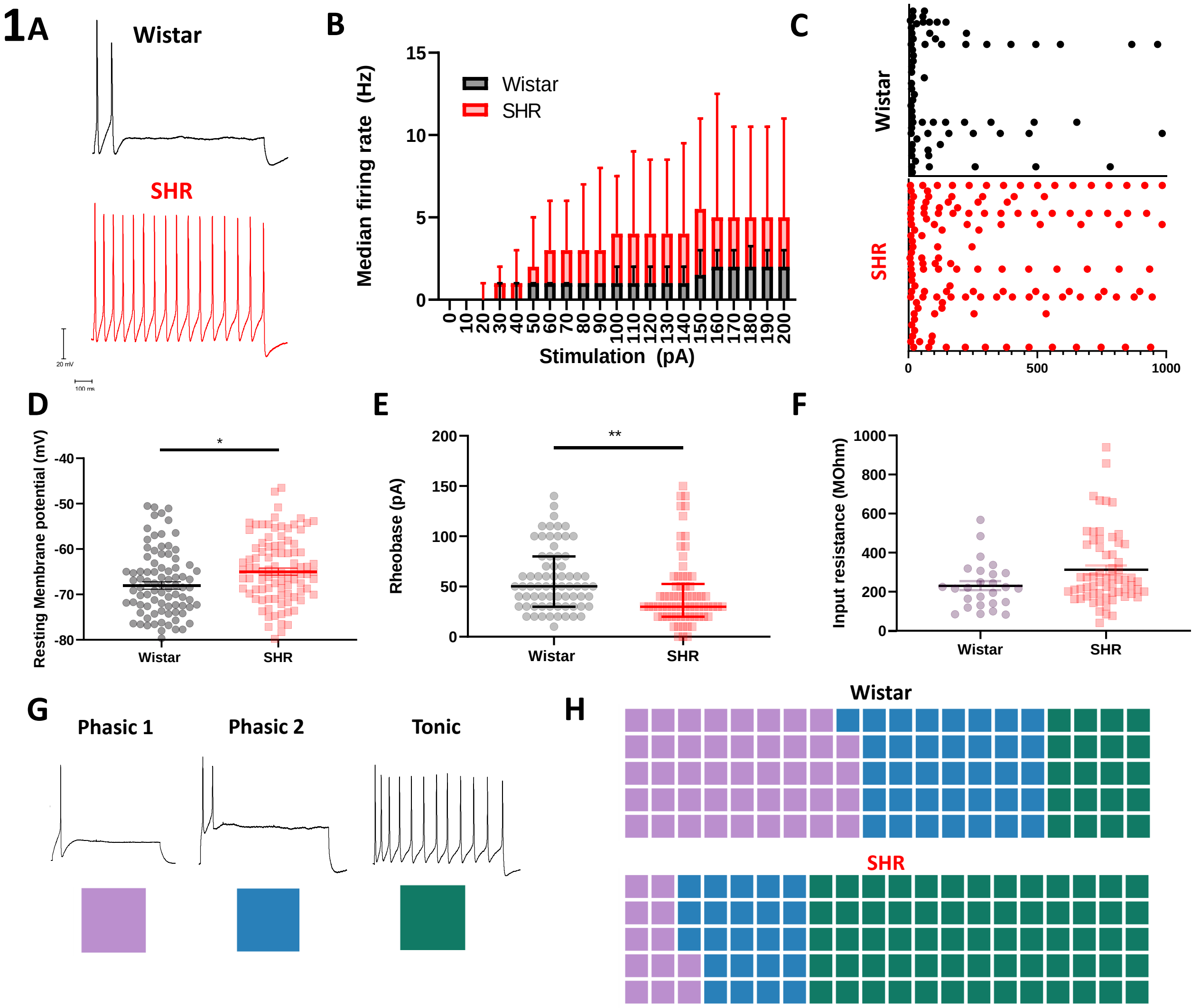
1A
Wistar
SHR
20 mV
100 ms
B
Median firing rate (Hz)
Wistar
SHR
Stimulation (pA)
C
Wistar
SHR
D
Resting Membrane potential (mV)
Wistar
SHR
E
Rheobase (pA)
Wistar
SHR
F
Input resistance (MOhm)
Wistar
SHR
G
Phasic 1
Phasic 2
Tonic
H
Wistar
SHR

2 A

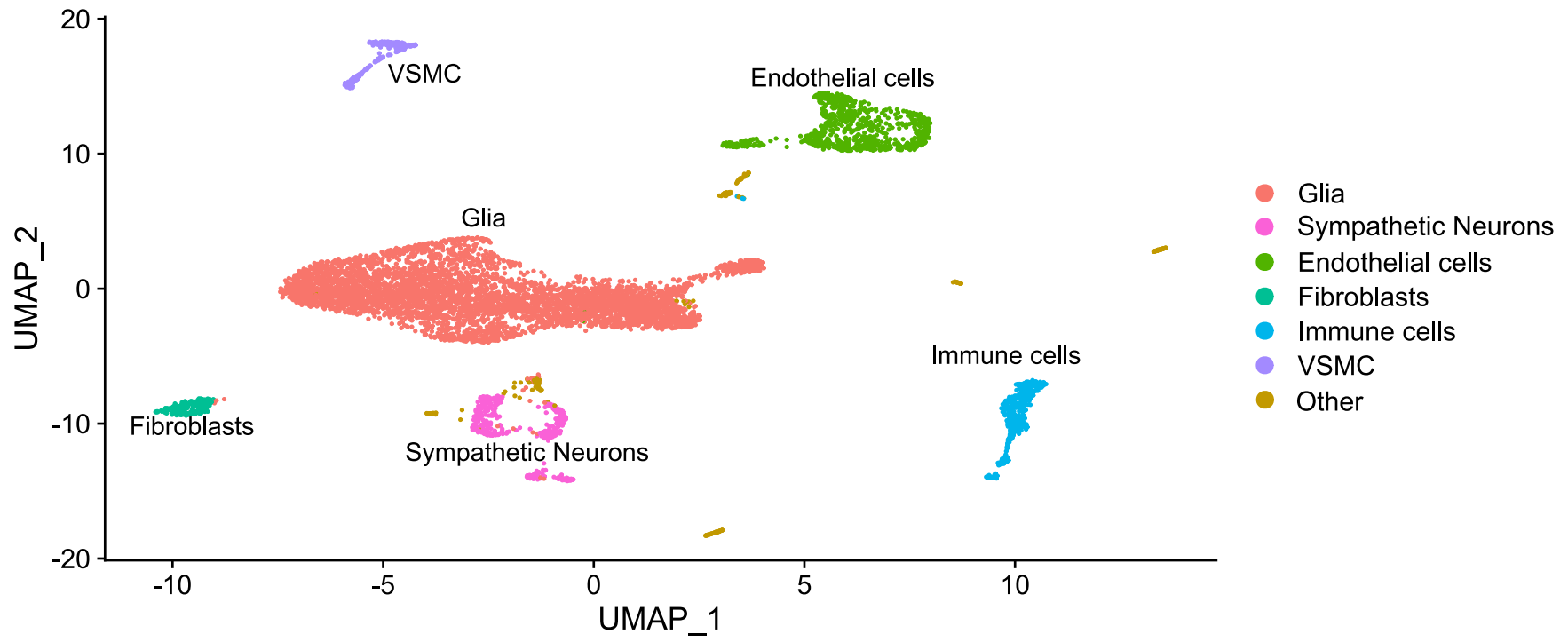
VSMC
Endothelial cells
Glia
Immune cells
Fibroblasts
Sympathetic Neurons
UMAP_2
UMAP_1
20
10
0
-10
-20
-10
-5
0
5
10
Glia
Sympathetic Neurons
Endothelial cells
Fibroblasts
Immune cells
VSMC
Other

B

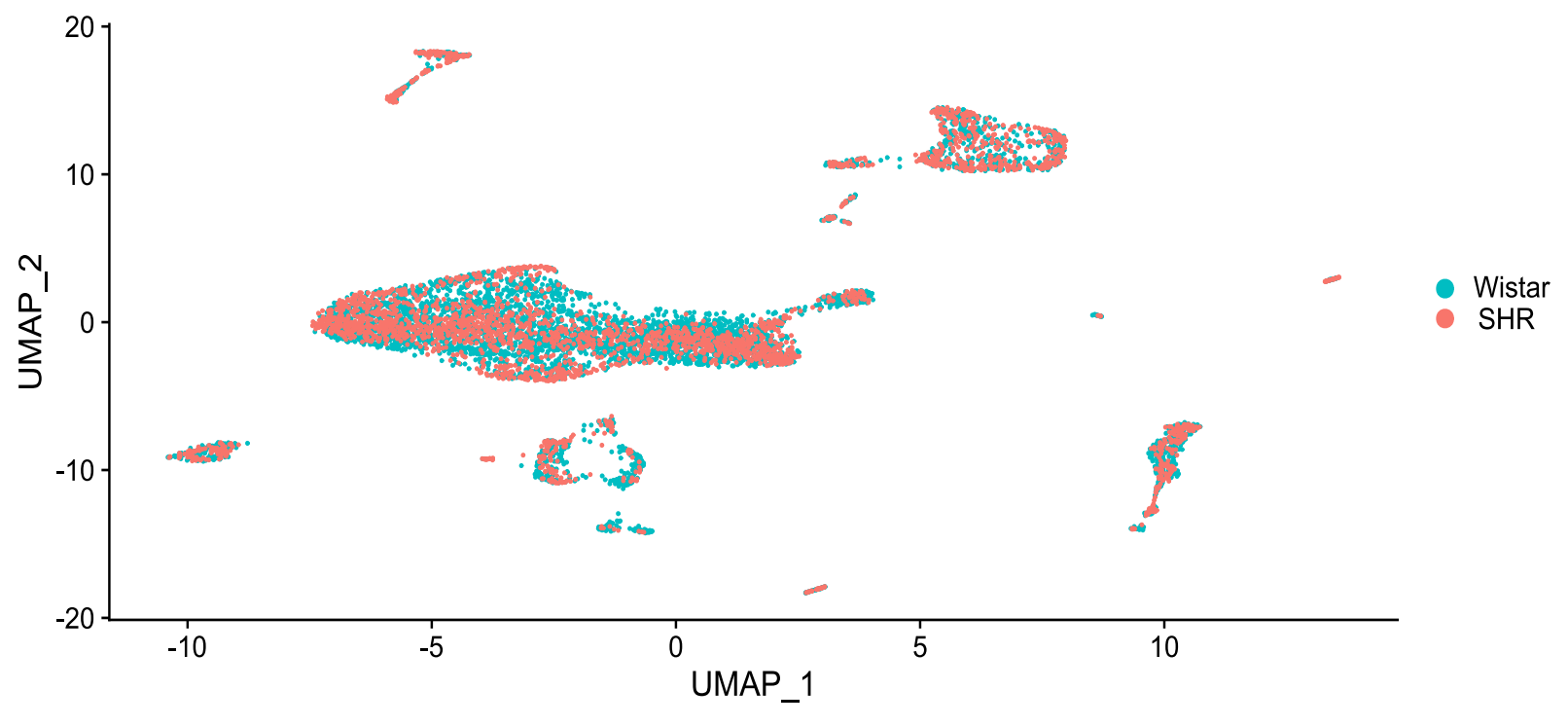
UMAP_2
UMAP_1
20
10
0
-10
-20
-10
-5
0
5
10
Wistar
SHR

C

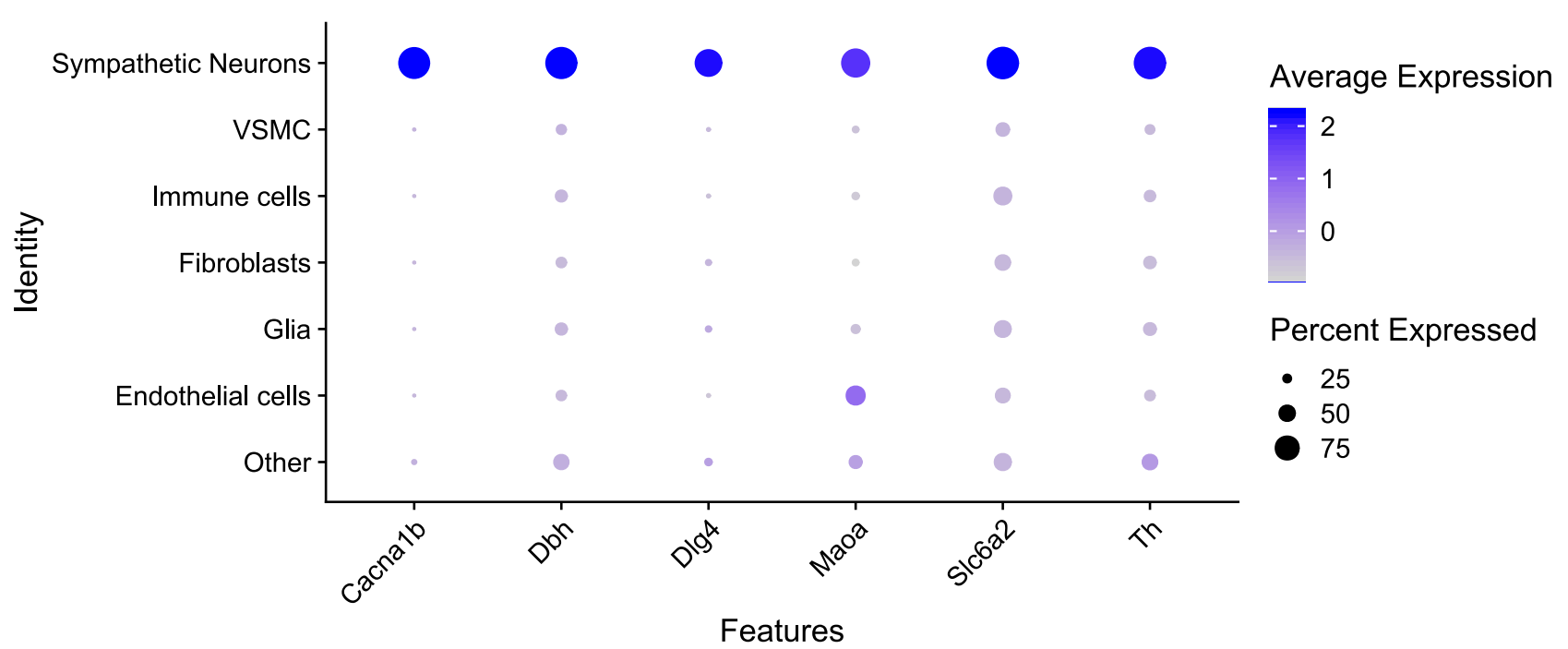
Sympathetic Neurons
VSMC
Immune cells
Fibroblasts
Glia
Endothelial cells
Other
Identity
Cacna1b
Dbh
Dlg4
Maoa
Slc6a2
Th
Features
Average Expression
2
1
0
Percent Expressed
25
50
75

Table 1

Gene	Fold change	Percentage Wistar	Percentage SHR	Adjusted P Value
Cacna1b	-0.48	0.98	0.98	1.67E-04
Kcnq5	-0.29	0.84	0.84	9.86E-06
Scn1a	-0.29	0.74	0.77	6.97E-02
Scn2a	-0.34	0.88	0.96	2.42E-03
Scn9a	-0.30	1	0.99	3.93E-07

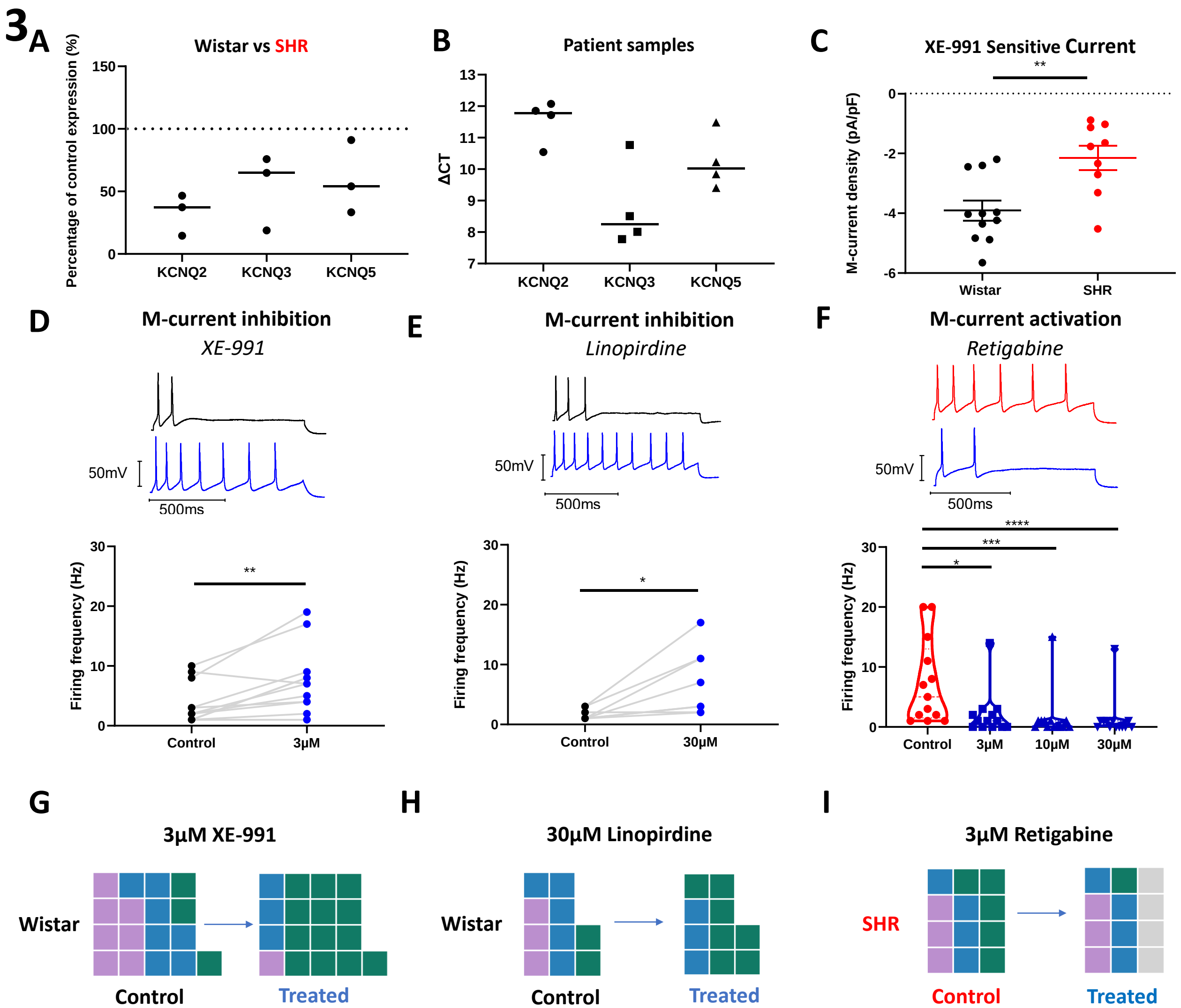
3
A
Wistar vs SHR
Percentage of control expression (%)
150
100
50
0
KCNQ2
KCNQ3
KCNQ5
B
Patient samples
ΔCT
13
12
11
10
9
8
7
KCNQ2
KCNQ3
KCNQ5
C
XE-991 Sensitive Current
**
M-current density (pA/pF)
0
-2
-4
-6
Wistar
SHR
D
M-current inhibition
XE-991
50mV
500ms
Firing frequency (Hz)
30
20
10
0
**
Control
3μM
E
M-current inhibition
Linopirdine
50mV
500ms
Firing frequency (Hz)
30
20
10
0
*
Control
30μM
F
M-current activation
Retigabine
50mV
500ms
****
***
*
Firing frequency (Hz)
30
20
10
0
Control
3μM
10μM
30μM
G
3μM XE-991
Wistar
Control
Treated
H
30μM Linopirdine
Wistar
Control
Treated
I
3μM Retigabine
SHR
Control
Treated

4

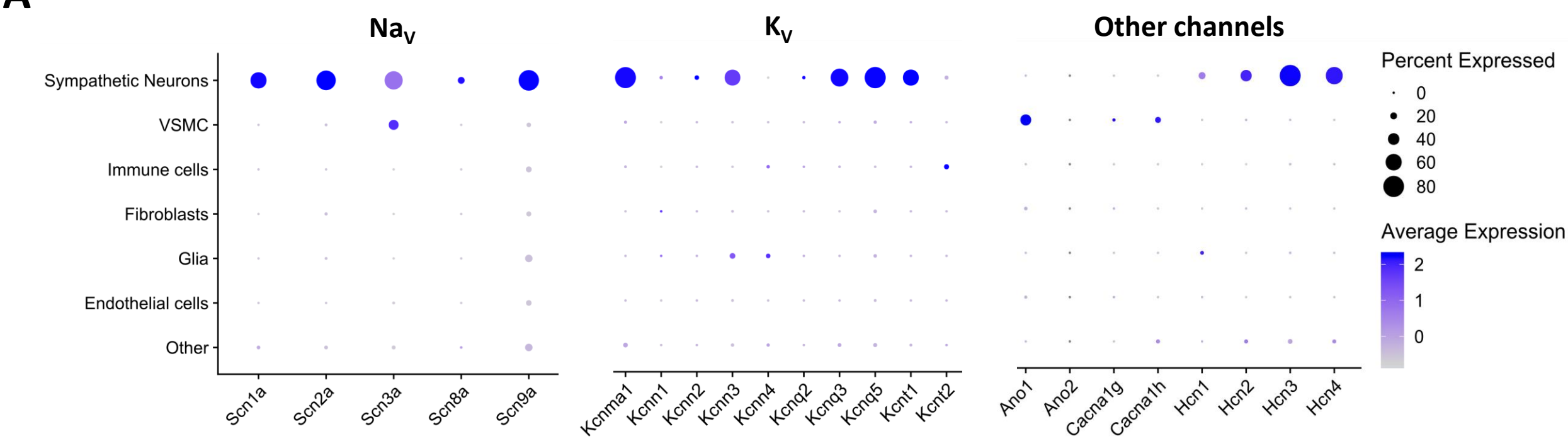
A
Na$_V$
K$_V$
Other channels
Sympathetic Neurons
VSMC
Immune cells
Fibroblasts
Glia
Endothelial cells
Other
Scn1a
Scn2a
Scn3a
Scn8a
Scn9a
Kcnma1
Kcnn1
Kcnn2
Kcnn3
Kcnn4
Kcnq2
Kcnq3
Kcnq5
Kcnt1
Kcnt2
Ano1
Ano2
Cacna1g
Cacna1h
Hcn1
Hcn2
Hcn3
Hcn4
Percent Expressed
0
20
40
60
80
Average Expression
2
1
0

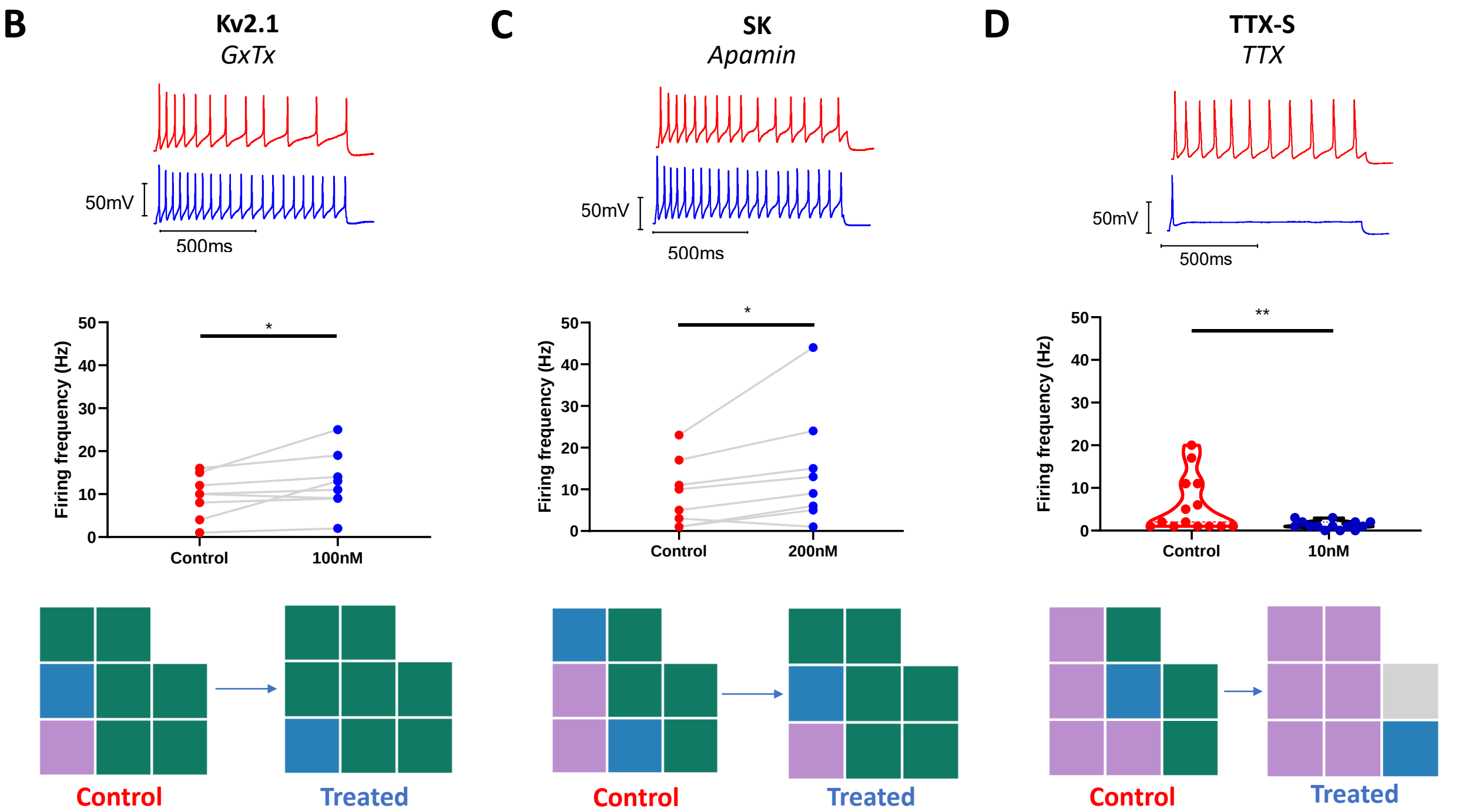
B
Kv2.1
GxTx
50mV
500ms
Firing frequency (Hz)
Control
100nM
C
SK
Apamin
50mV
500ms
Firing frequency (Hz)
Control
200nM
D
TTX-S
TTX
50mV
500ms
Firing frequency (Hz)
Control
10nM
Control
Treated
Control
Treated
Control
Treated

5

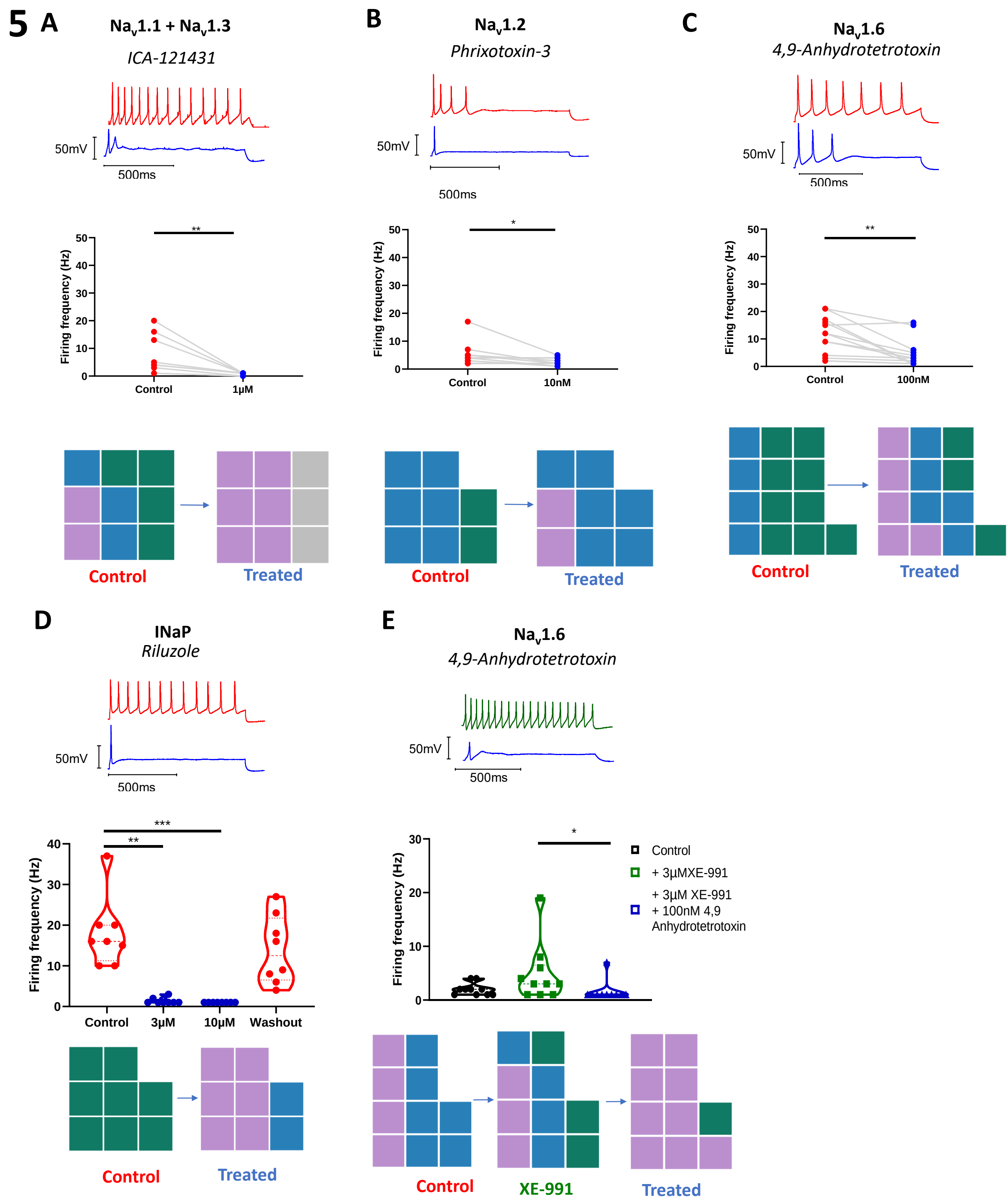
A
Na$_v$1.1 + Na$_v$1.3
ICA-121431
50mV
500ms
Firing frequency (Hz)
Control
1µM
B
Na$_v$1.2
Phrixotoxin-3
50mV
500ms
Control
10nM
C
Na$_v$1.6
4,9-Anhydrotetrotoxin
50mV
500ms
Control
100nM
Control
Treated
D
INaP
Riluzole
50mV
500ms
Control
3µM
10µM
Washout
E
Na$_v$1.6
4,9-Anhydrotetrotoxin
50mV
500ms
Control
+ 3µMXE-991
+ 3µM XE-991
+ 100nM 4,9
Anhydrotetrotoxin
XE-991

Table 2

	HCN		T-type		Ca2+ free	BK	CaCC	Nav1.7		KNa
Drug	Ivabradine	ZD7288	TTA-A2	TTA-P2	EGTA	Iberiotoxin	Ani9	Protx-III	Huwentoxin-IV	Lithium
Concentration	3µM	1µM	500nm	1µM	5mM	100nM	1µM	50nM	50nM	N/A
Perforating agent	Amphotericin	Amphotericin	Amphotericin	Amphotericin	Amphotericin	Amphotericin	Amphotericin	Amphotericin	Amphotericin	Whole cell
Δ Firing rate 150pA	-1	0	0	-1	-1	0	0.5	0	2.5	0
P value	*0.67*	*0.5*	*>0.99*	*0.60*	*0.59*	*0.81*	*0.87*	*0.38*	*0.11*	*0.84*
Δ Firing rate 100pA	0	0.5	0	-0.5	1.000	0	0.5	0	0.5	0
P value	*0.75*	*0.95*	*0.25*	*0.89*	*0.22*	*0.9414*	*0.5469*	*0.44*	*0.19*	*0.5*
Δ Firing rate 50pA	0	0.5	1	0	0	0	0.5	-0.5	0	0
P value	*0.19*	*0.25*	*0.16*	*>0.99*	*0.094*	*>0.9999*	*0.5156*	*0.63*	*0.5*	*0.25*
Δ Maximum firing rate	0	0	0	-0.5	0.5	0	1	-0.5	1	0
P Value	*0.13*	*>0.99*	*0.63*	*0.51*	*0.61*	*0.60*	*0.29*	*0.67*	*0.19*	*0.81*
n	10	8	9	10	12	12	10	8	8	10

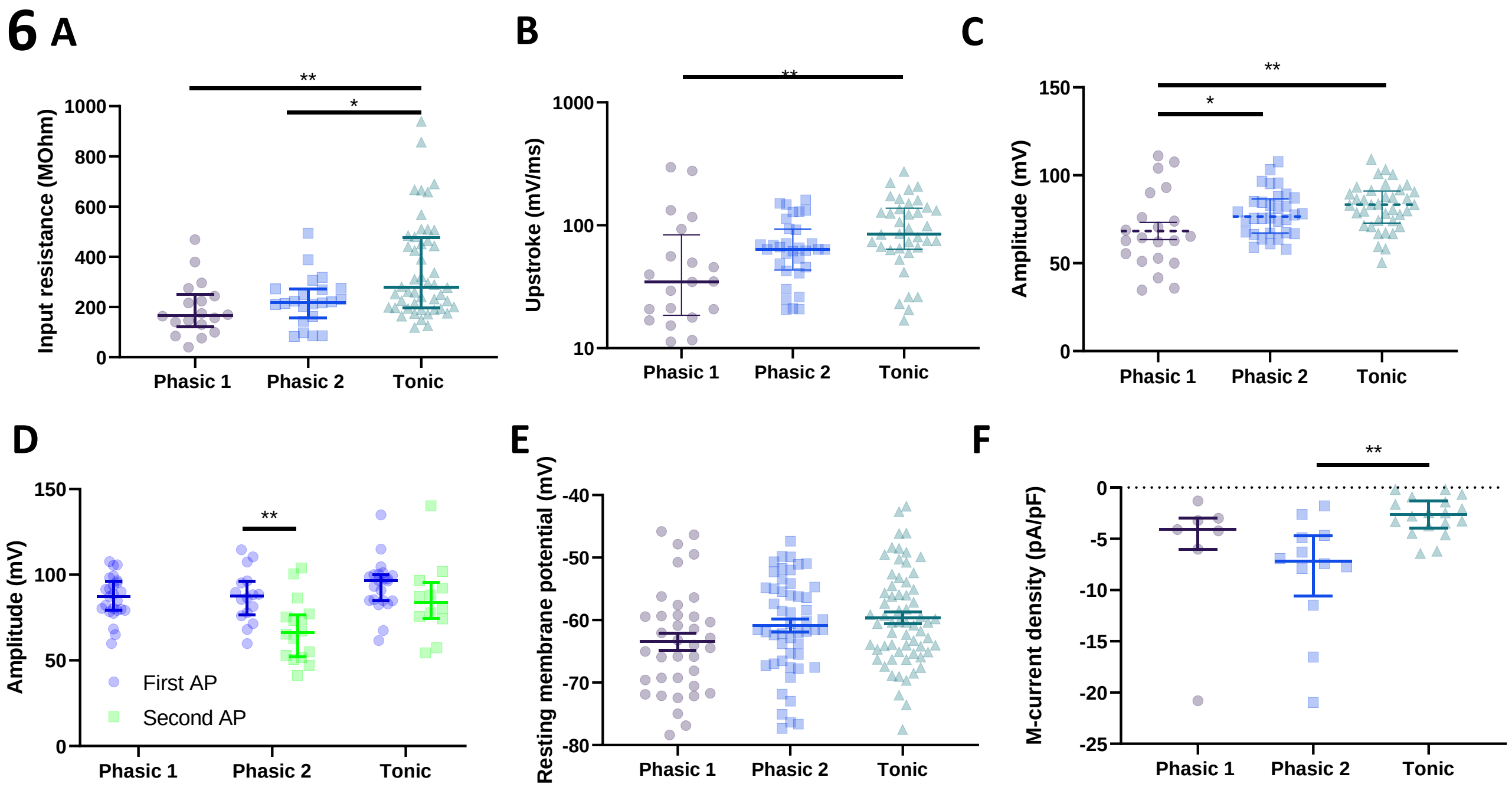
6
A
B
C
D
E
F
Input resistance (MOhm)
Upstroke (mV/ms)
Amplitude (mV)
Resting membrane potential (mV)
M-current density (pA/pF)
Phasic 1
Phasic 2
Tonic
First AP
Second AP
**
*

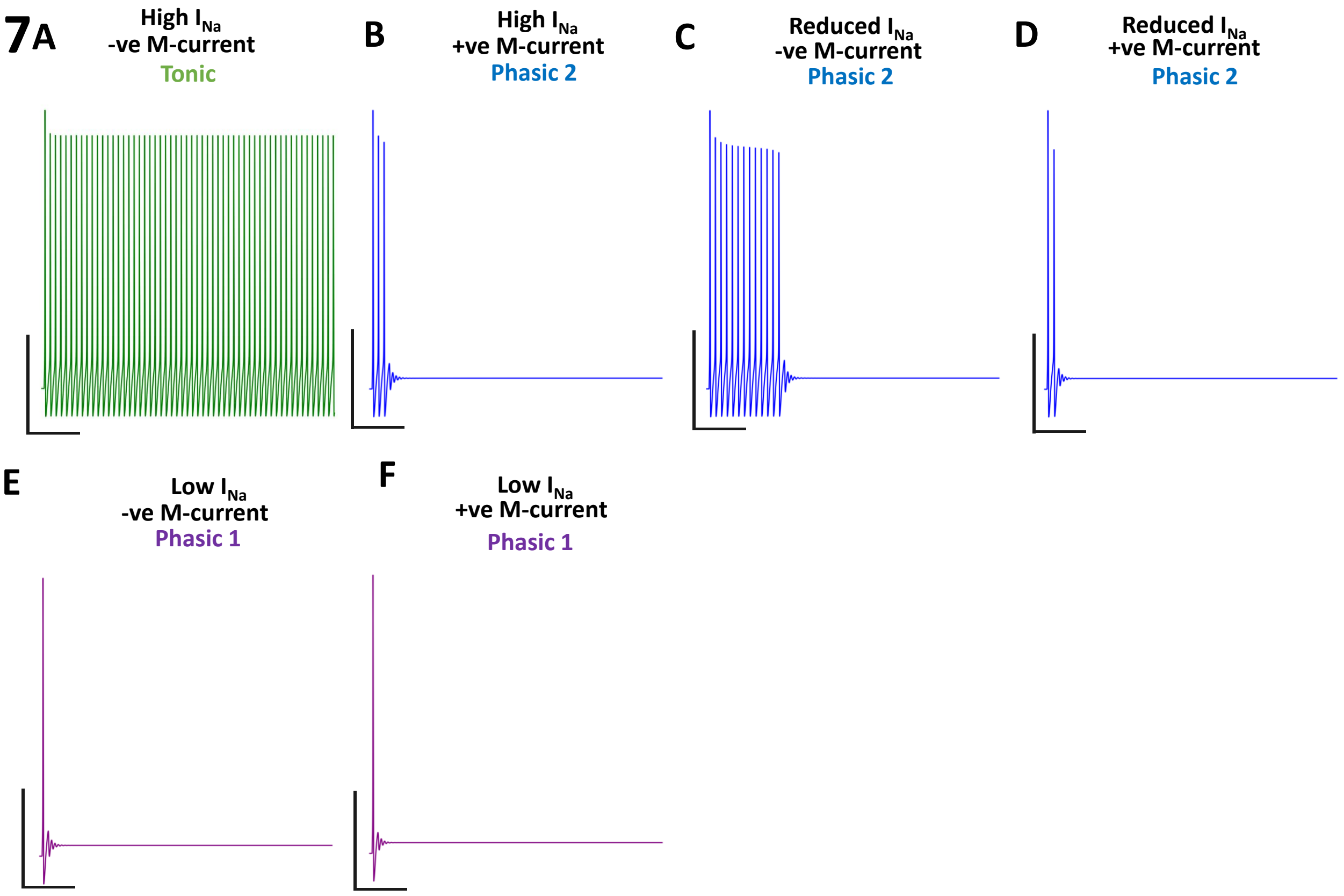
7A
High I_{Na}
-ve M-current
Tonic
B
High I_{Na}
+ve M-current
Phasic 2
C
Reduced I_{Na}
-ve M-current
Phasic 2
D
Reduced I_{Na}
+ve M-current
Phasic 2
E
Low I_{Na}
-ve M-current
Phasic 1
F
Low I_{Na}
+ve M-current
Phasic 1